Received: 27 January 2021 | Revised: 12 May 2021 | Accepted: 27 May 2021

DOI: 10.1002/inf2.12220

REVIEW ARTICLE

WILEY

Piezotronics in two-dimensional materials

Qin Zhang[1,2] | **Shanling Zuo**[1] | **Ping Chen**[1,2] | **Caofeng Pan**[1,2,3]

[1]Center on Nanoenergy Research, Guangxi Key Laboratory for Relativistic Astrophysics, School of Physical Science and Technology, Guangxi University, Nanning, China

[2]CAS Center for Excellence in Nanoscience, Beijing Key Laboratory of Micro-Nano Energy and Sensor, Beijing Institute of Nanoenergy and Nanosystems, Chinese Academy of Sciences, Beijing, China

[3]School of Nanoscience and Technology, University of Chinese Academy of Sciences, Beijing, China

Correspondence
Ping Chen and Caofeng Pan, Center on Nanoenergy Research, Guangxi Key Laboratory for Relativistic Astrophysics, School of Physical Science and Technology, Guangxi University, Nanning 530004, China.
Email: chenping@gxu.edu.cn and cfpan@binn.cas.cn

Funding information
Fundamental Research Funds for the Central Universities; National Key R&D Project from Minister of Science and Technology, China, Grant/Award Number: 2016YFA0202703; National Natural Science Foundation of China, Grant/Award Numbers: 11704081, U20A20166, 61675027, 61805015, 618040; Natural Science Foundation of Beijing Municipality, Grant/Award Number: Z180011; Natural Science Foundation of Guangxi Province, Grant/Award Numbers: 2020GXNSFAA297182, 2017GXNSFBA198229; Shenzhen Science and Technology Program, Grant/Award Number: KQTD20170810105439418

Abstract

The fascinating two-dimensional (2D) materials are being potentially applied in various fields from science to engineering benefitting from the charming physical and chemical properties on optics, electronics, and magnetism, compared with the bulk crystal, while piezotronics is a universal and pervasive phenomenon in the materials with broking center symmetry, promoting the new field and notable achievements of piezotronics in 2D materials with higher accuracy and sensitivity. For example, 20 parts per billion of the detecting limitations in NO_2 sensor, 500 μm of spatial strain resolution in flexible devices, and 0.363 eV output voltage in nanogenerators. In this review, three categories of 2D piezotronics materials are first introduced ranging from organic to inorganic data, among which six types of 2D inorganic materials are emphasized based on the geometrical arrangement of different atoms. Then, the microscopic mechanism of carrier transport and separation in 2D piezotronic materials is highlighted, accompanied with the presentation of four measured methods. Subsequently, the developed applications of 2D piezotronics are discussed comprehensively including different kinds of sensors, piezo-catalysis, nanogenerators and information storage. Ultimately, we suggest the challenges and provide the ideas for qualitative–quantitative research of microscopic mechanism and large-scale integrated applications of 2D piezotronics.

KEYWORDS

carrier transport, flexible devices, piezotronics, two-dimensional materials

1 | INTRODUCTION

Piezotronics, regulating the carrier transport by piezo-potential,[1–4] has received significant attentions and substantial expansion for intrinsic applications in piezoelectric, piezophototronics, and flexible devices due to the universality and pervasiveness of internal and external strain in the devices and non-center symmetrical semiconductors.[5–12] Simultaneously, two-dimensional (2D) materials were widely explored on optics,[13–24] electronics,[25–33] and magnetism.[34–41] since the first discovery of single atomic thickness graphene. Thus, piezotronics based on 2D materials was presented and developed rapidly from microscopic mechanism, various materials to the practical applications on nanogenerators, sensors, catalysis, information storage, and other flexible devices.[42–54]

The entrance of piezotronics from 2D materials was opened thoroughly since the first experimental confirmation from 2D MoS_2 by Hone and Wang groups in 2014, where piezo-voltage and output current were detected only from MoS_2 flakes with odd number of atomic layers.[31] Then, piezotronics based on 2D materials has been grown into forest since the expansion from black phosphorus (BP),[55–59] hexagonal boron nitride (h-BN),[60–63] transition metal dichalcogenide (TMDCs) and Janus TMDCs,[63–72] II-VI semiconductors,[73–79] III-V,[80–88] Group-III monochalcogenides (III-VI),[89,90] and Janus III-VI,[91,92] Group-IV monochalcogenides (IV-VI),[93–97] Group-V (V-V),[98] and so on.[99–109] At the same time, the variety of applications of piezotronics from 2D materials were achieved on flexible optoelectronics, piezotronic catalysis, biological medicine, information storage, and so forth.

Herein, we introduce three categories of 2D materials for piezotronics at first, where six kinds of inorganic crystals are distinguished according to the composition and structure of monolayer materials. Then, the reported methods for detecting piezotronic signal and mechanism of 2D piezotronics are concluded and discussed. Additionally, the applications, evolvement, and presented problems are revealed and proposed to promote the advancement of various sensors, nanogenerators, piezo-catalysis and information storage. Finally, the challenges and visions are furnished to expand the depth and breadth of 2D piezotronics. This review is aimed at providing a top view of the development, problem, and prospect of piezotronics in 2D materials.

2 | 2D MATERIALS FOR PIEZOTRONICS

Piezotronics is presented in the materials with centro-symmetric breaking, where the centers of gravity from the cations and anions are not coincided when applied an external strain, leading to the generation of piezo-potential in the interface between the semiconductors and the metals. The piezo-potential will modulate the Schottky barrier height (SBH) and output current passing through the interface, resulting in the enhanced or weakened sensitivity factor.[75] Therefore, 2D materials with non-center symmetry structure have the potential for exploiting piezotronics. We divide the reported 2D materials for piezotronics into three categories: 2D inorganic materials with non-center symmetry structure originally, modulated 2D materials who possess center symmetry structure originally, and 2D organic perovskites.

2.1 | 2D inorganic materials

Reed group calculated and predicted the piezotronic monolayer materials among 1173 2D layer materials from the materials project database with more than 50 000 inorganic crystals.[106] 325 monolayer 2D crystals were identified to be potential 2D piezotronic materials, which lack the center symmetry structure originally. And the reported 2D monolayer piezotronic materials currently can be classified into six categories according to the crystal structure, containing TMDCs and Janus TMDCs, II-VI, III-V, III-VI and Janus III-VI, IV-VI, and V-V (Figures 1 and 2).

2.1.1 | TMDCs and Janus TMDCs

Monolayer TMDCs are usually marked as MX_2, where M represents transition metal elements and X indicates chalcogen atoms.[63–65] Monolayer piezotronic TMDCs have the hexagonal crystal structure and D_{3h} symmetry with the space group $p\bar{6}m2$.[64,71,110] Density functional theory was calculated and the experiment was performed to confirm the piezoelectric coefficient and bandgap of TMDCs to be the range of 2.12–13.54 pm V^{-1},[63–65,70] and 0.52–2.1 eV,[8,65,66,111] respectively (Figure 2A). Meanwhile, the piezoelectric coefficient of TMDCs is increased with increasing the atomic number of chalcogen atoms or decreasing the atomic number of transition metal atoms.[64]

Janus TMDCs are used to be presented as MXY, where $X \neq Y$, M is transition metal elements, X and Y indicate chalcogen atoms.[67,71,112] For different atomic radius and electronegativities of X and Y atoms, bond lengths from M-X and M-Y are different from each other and symmetry along vertical direction is broken, resulting in a lower symmetry than monolayer TMDCs. The site symmetry and space group of monolayer Janus TMDCs are C_{3v} and *P3m1*,[71,92,112] respectively. The range of piezoelectric coefficients of in-plane (d_{11}) and out-of-plane (d_{31}) are 2.26–5.30 pm V^{-1} and 0.007–0.30 pm V^{-1},[71,92] respectively.

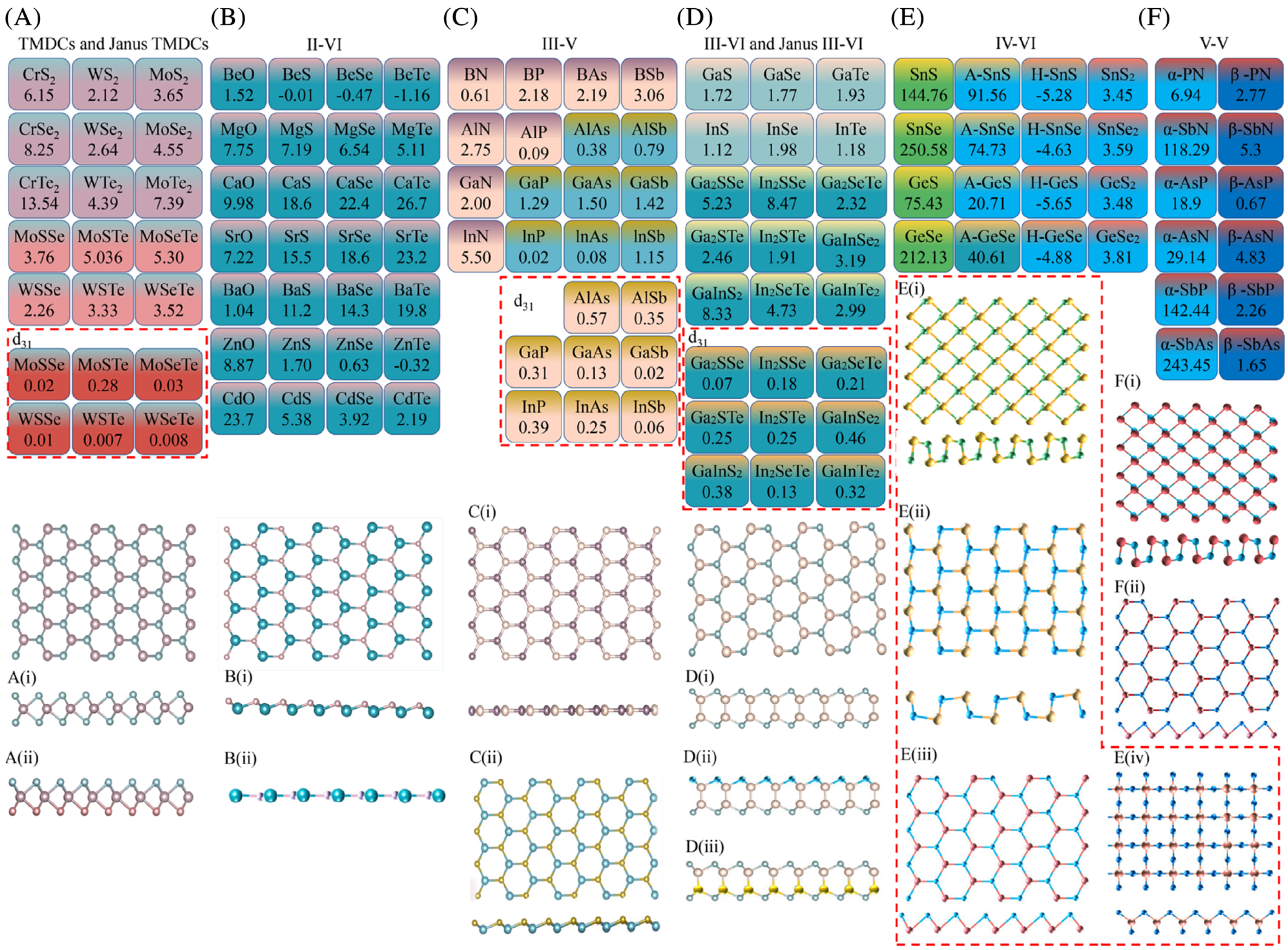

FIGURE 1 Piezoelectric coefficients and crystal structures of monolayer TMDCs and Janus TMDCs (A), II-VI (B), III-V (C), III-VI and Janus III-VI (D), IV-VI (E), V-V (F)

2.1.2 | II-VI

Monolayer II-VI semiconductors are expressed as MX, where M is II atoms and X is VI atoms.[79] Monolayer II-VI semiconductors have a honeycomb structure with non-centrosymmetric atom arrangement.[77,78] Piezoelectric coefficient and bandgap of monolayer II-VI were calculated to be the range of −1.16 to 26.7 pm V^{-1},[70,73,79] and 0.66–5.34 eV,[76–78] respectively (Figure 2B). Piezoelectric coefficients were predicted to be enhanced by decreasing the atomic number of M (M = Ba, Mg, Zn, Cd) or increasing the atomic number of M atoms (M = Ca, Sr, Ba).[63,73,79]

2.1.3 | III-V

Monolayer III-V semiconductors are also shown as MX, where M is III atoms and X is V atoms.[86] The crystal structure can be divided into in-plane hexagonal and non-plane hexagonal, where those with in-plane structure are stable in the air. The space group and symmetry of monolayer III-V with in-plane structure are $p\bar{6}m2$ and D_{3h},[80,81,86] respectively (Figure 1C, i). And the piezoelectric coefficient and bandgap of monolayer III-V are from 0.09 to 5.5 pm V^{-1},[63,84] and 0.31 to 5.9 eV,[81,84] respectively (Figure 2C,D). While the space group and symmetry of III-V semiconductors with non-plane structure are $Pmn2_1$ and C_{2v}.[80,85] For the non-plane structure, the piezoelectric coefficient of monolayer III-V semiconductors has two kinds: in parallel (d_{11}) and perpendicular (d_{31}) planes, which are in the scope of 0.02–1.50 pm V^{-1} and 0.02–0.57 pm V^{-1}, respectively.[63,82,84] The bandgap is 0.74–2.49 eV.[81,83,85] Besides, the piezoelectric coefficients of d_{11} and d_{31} increase with decreasing the atomic number of V atoms or increasing the atomic number of III atoms except for AlN, GaN, and InN.

2.1.4 | III-VI and Janus III-VI

III-VI semiconductors can be represented as MX or MMXX (M = Ca, In; X = S, Se, Te). Space group and

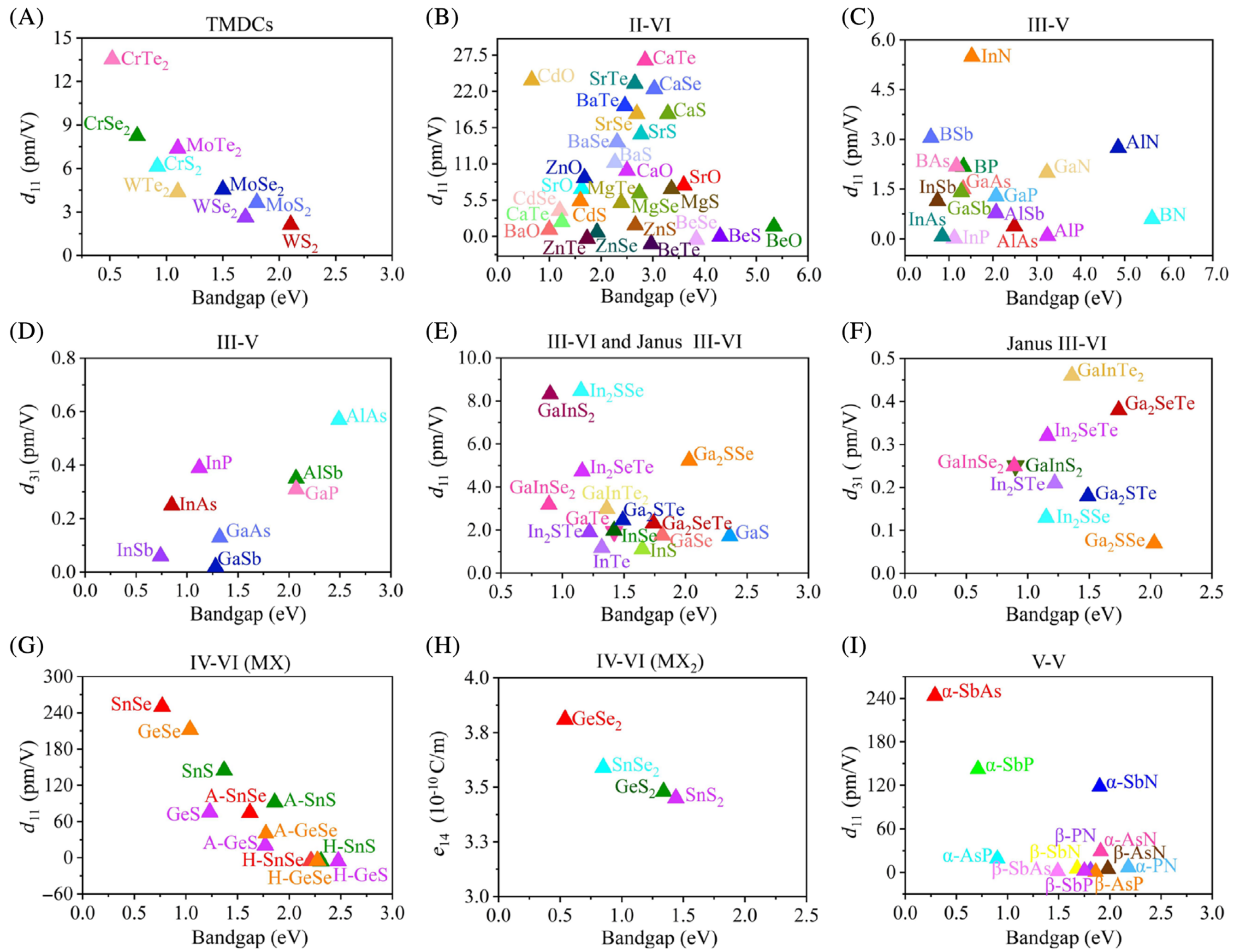

FIGURE 2 Piezoelectric coefficients and bandgap of monolayer TMDCs (A), II-VI (B), III-V (C,D), III-VI and Janus III-VI (E,F), IV-VI (G,H), V-V (I)

symmetry belong to $p\bar{6}m2$ and D_{3h}, respectively.[89] The piezoelectric coefficient of d_{11} is in the range of 1.12–1.98 pm V^{-1}.[70,87] The bandgap is from 1.32 to 2.36 eV.[91,92] When M or X is replaced by other atoms, III-VI becomes Janus III-VI, termed as M_2XX' or $MM'X_2$ (M, M′ = Ca, In; X, X′ = S, Se, Te).[91] Janus III-VI belongs to layered hexagonal structure with site symmetry D_3.[91] The piezoelectric coefficients of d_{11} and d_{31} are from 1.91 to 8.47 pm V^{-1} and from 0.07 to 0.46 pm V^{-1}, respectively.[91,92] And the bandgap is from 0.89 to 2.03 eV (Figure 2E,F).[91,92]

2.1.5 | IV-VI

Four types of structures are contained in monolayer IV-VI semiconductors, which are indicated by MX or MX_2 (M = Sn, Ge; X = Se, S). For the presentation of MX, puckered or hexagonal crystal structures were reported (Figure 1E, i–iii). One of the puckered structures is alternated by the zigzag line (Figure 1E, i), like black phosphorene, with C_{2v} site symmetry and $Pmn2_1$ space group,[80,95,96] And piezoelectric coefficient d_{11} and bandgap of this MX are 75.43–250.28 pm V^{-1} and 0.77–1.37 eV.[94] The other puckered structure of MX shows a rectangular Wigner-Seitz cell alternated by the armchair direction with piezoelectric coefficient d_{11} and bandgap in the range of 20.7–91.56 pm V^{-1} and 1.62–1.86 eV (Figure 1E, ii). Simultaneously, the MX with hexagonal structure (Figure 1E, iii) presents that piezoelectric coefficient d_{11} and bandgap are from −5.65 to −4.63 pm V^{-1} and 2.21 to 2.47 eV,[96] respectively. While MX_2 shows D_{2d} site symmetry and $p\bar{4}m2$ space group (Figure 1E, iv).[95,97] The piezoelectric coefficient e_{14} and bandgap of MX_2 are 3.45–3.81 × 10^{-10} C m^{-1} and 0.54–1.44 eV (Figure 2G,H).[97]

2.1.6 | V-V

Monolayer V-V semiconductors possess α-phase and β-phase induced by their flexible structures and special symmetry.[113] The space group and symmetry of α-phase and β-phase are calculated to be C_{2v}, $Pmn2_1$ and C_{3v}, $P3m1$,[80,98] respectively. The piezoelectric coefficient d_{11} and bandgap of α-phase are 6.94–243.45 pm V^{-1} and 0.29–2.18 eV,[98] while those of β-phase are 0.67–4.83 pm V^{-1} and 1.49–1.98 eV (Figure 2I).[98] Both piezoelectric coefficients d_{11} from α-phase and β-phase of V-V materials increase with increasing the atomic number of V cation.

2.2 | Modulated 2D materials

The piezotronic engineering has been developed in graphene-like 2D materials by modulating the interfaces or defects in 2D materials, which possess a center symmetric structure originally. Three techniques were explored for changing center symmetric structure to non-center symmetry: interface interaction,[114] atomic adsorption,[115–122] and introducing defects (Figure 3).[123,124]

The 2D materials with center symmetry structure originally could generate piezo-response with the modulation from interfaces. Kholkin group observed piezotronic response in graphene with the chemical interaction

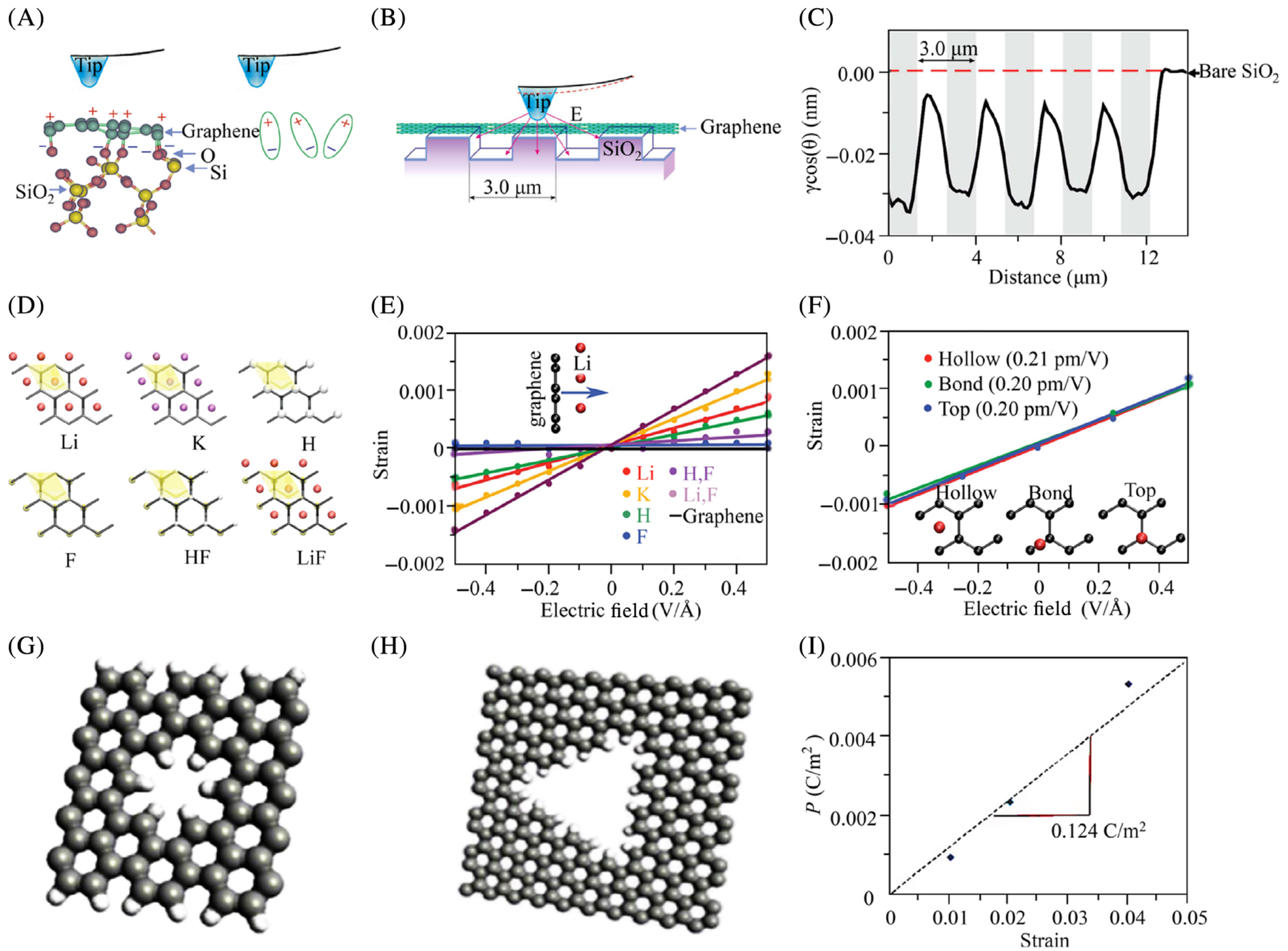

FIGURE 3 A, Schematic diagram of the piezoelectric activity of monolayer graphene on the SiO_2 substrate. B,C, Schematic of the PFM measurement and piezo-response of graphene supported on SiO_2 substrate and suspended graphene. Reproduced with permission.[114] Copyright 2015, spring nature. D, Schematic diagram of different absorbed atoms on graphene. E, Dependence of equibiaxial strain on electric field for different absorbed position of Li^+ on graphene. F, Dependence of equibiaxial strain on electric field for different absorbed atoms on graphene. Reproduced with permission.[116] Copyright 2012, American Chemical Society. G,H, Schematic of circular (G) and triangular (H) defects in graphene. I, Dependence polarization on the external strain of graphene with triangular defects. Reproduced with permission.[123] Copyright 2012, American Institute of Physics

between graphene and oxygen atoms from SiO_2 substrate (Figure 3A–C).[114] The piezo-response from graphene supported by SiO_2 substrate is four times than that of suspended one, indicating the interaction between graphene and substrate induces the change of interface properties of graphene, which leads to non-center symmetry and piezotronic material of graphene.

Selective surface adsorption of atoms on non-piezotronic graphene could also break center symmetry and generate piezotronic effects. Reed group found absorbed Li^+ atoms on graphene could produce non-center symmetric graphene and piezo-response (Figure 3D–F).[116] The absorbed position on graphene does not affect the piezoelectric coefficient significantly. While the species of absorbed atoms has a strong influence on the piezoelectric coefficient d_{31}.

Non-center symmetric internal defects in graphene can induce piezotronic effect simultaneously. Sharma et al. introduced circular and triangular defects in graphene by electron beam irradiation (Figure 3G–I).[123] The graphene with circular defect does not show piezo-response, while that with triangular defects gives a piezoelectric coefficient of 0.124 C m^{-2}. Then, Kelany et al. built two hole-like defects in monolayer graphene with changing the symmetry of graphene from D_{6h} into D_{3h} and C_{2v}, respectively.[118] Both types of defects present the piezoelectric response, where the piezoelectric value is as large as $5.6 \pm 0.4 \times 10^{-10}$ C m^{-1}.

2.3 | 2D organic–inorganic hybrid perovskites

Organic–inorganic hybrid perovskites have developed into a new type of 2D piezotronic material.[125–133] The organic–inorganic hybrid perovskites have already made into monolayer 2D sheets in 2015 (Figure 4A,B).[125] Mitzi group first detected the piezo-response from $(PMA)_2PbBr_4$, $(PEA)_2PbI_4$, $(NMA)_2PbBr_4$, $(NEA)_2PbI_4$, and $(NEA)_2PbBr_4$ by piezo-response force microscopy (PFM) and confirmed the non-center symmetric structure of those organic–inorganic hybrid perovskites (Figure 4C).[126] Then, Xiong group measured the piezo-amplitude from $(ATHP)_2PbBr_4$

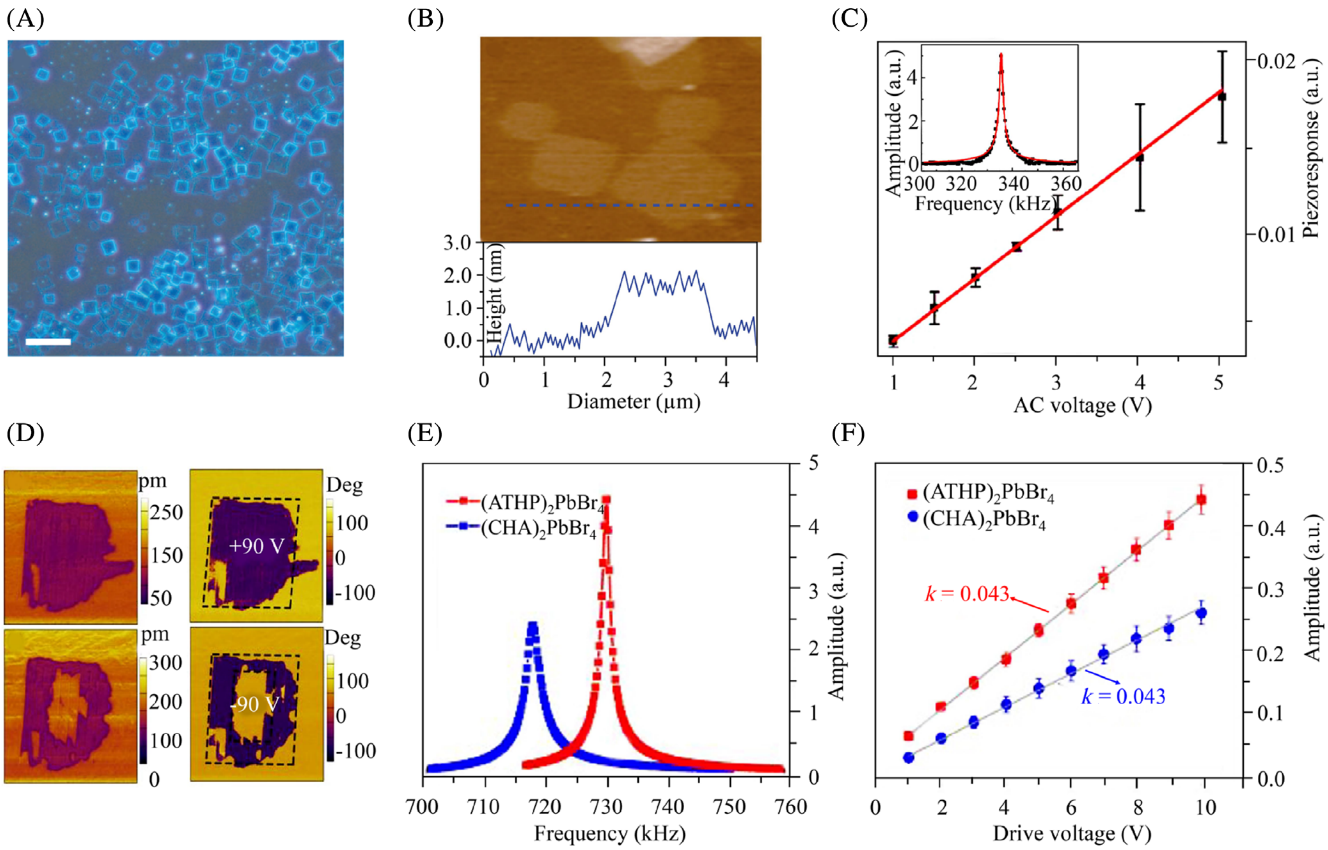

FIGURE 4 A,B, Optical (A) and AFM image (B) of monolayer $(C_4H_9NH_3)_2PbBr_4$ perovskites. Reproduced with permission.[125] Copyright 2015, American Association for the Advancement of Science. C, Schematic diagram illuminates piezo-response on driving voltage and frequency (inset). Reproduced with permission.[126] Copyright 2017, American Chemical Society. D, PFM images of $(ATHP)_2PbBr_4$. E,F, PFM resonance frequency (E) and piezoelectric amplitude (F) of $(ATHP)_2PbBr_4$ and $(CHA)_2PbBr_4$. Reproduced with permission.[127] Copyright 2020, American Chemical Society

and $(CHA)_2PbBr_4$ perovskites and confirmed the broken inversion symmetry by second harmonic generation (SHG).[127] In short, organic–inorganic hybrid perovskites are being explored as a new 2D piezotronic material.

3 | BASICS OF PIEZOTRONICS FOR 2D MATERIALS

Experimental measurement of piezo-response of 2D materials is important for developing piezotronics of 2D materials. Four methods have been reported to detect piezo-response: bending and releasing of flexible devices,[31,134–136] atomic force microscopy (AFM),[137–142] PFM,[143–148] and lateral excited scanning probe microscopy (SPM) (Figure 5A–D).[36,52,149]

The mechanism of piezotronics from 2D materials is similar to the modulated output current through the interfaces between metal and semiconductor,[31,44,150–154] or p-n junction.[44,155–157] For the interface between metal and semiconductor, we take n-type semiconductor for example (Figure 5E,F), where Schottky contact is created. The output current is decided by the SBH, which is modulated by the piezo-potential. The piezo-potential is induced by the center deviation of positive and negative charges when applied the external strain.[158] The negative piezo-potential around the interface increases the SBH and decreases the output current, while the positive piezo-potential around the interface reduces the SBH and enhances the output current, when applied external strain.[44] On the other hand, for the interface of p-n junction (Figure 5G,H), we take n-type 2D materials as the piezotronic materials. The negative piezo-potential repels electrons and increases the energy band height in n-type interface, resulting in broadening the depletion zone in n-type semiconductor and reducing the output current. While the positive piezo-potential attracts electrons and reduces the energy band height in n-type interface, leading to narrowing the depletion zone in n-type semiconductor and enhancing current when applied the external strain.[44]

4 | APPLICATIONS OF PIEZOTRONICS FROM 2D MATERIALS

According to the mechanism of piezotronics from 2D materials, the output current will be regulated to increase or decrease when applied the external strain. Thus, the gauge factor for related sensors will be enhanced or reduced, causing scrambling research of diverse applications, such as various

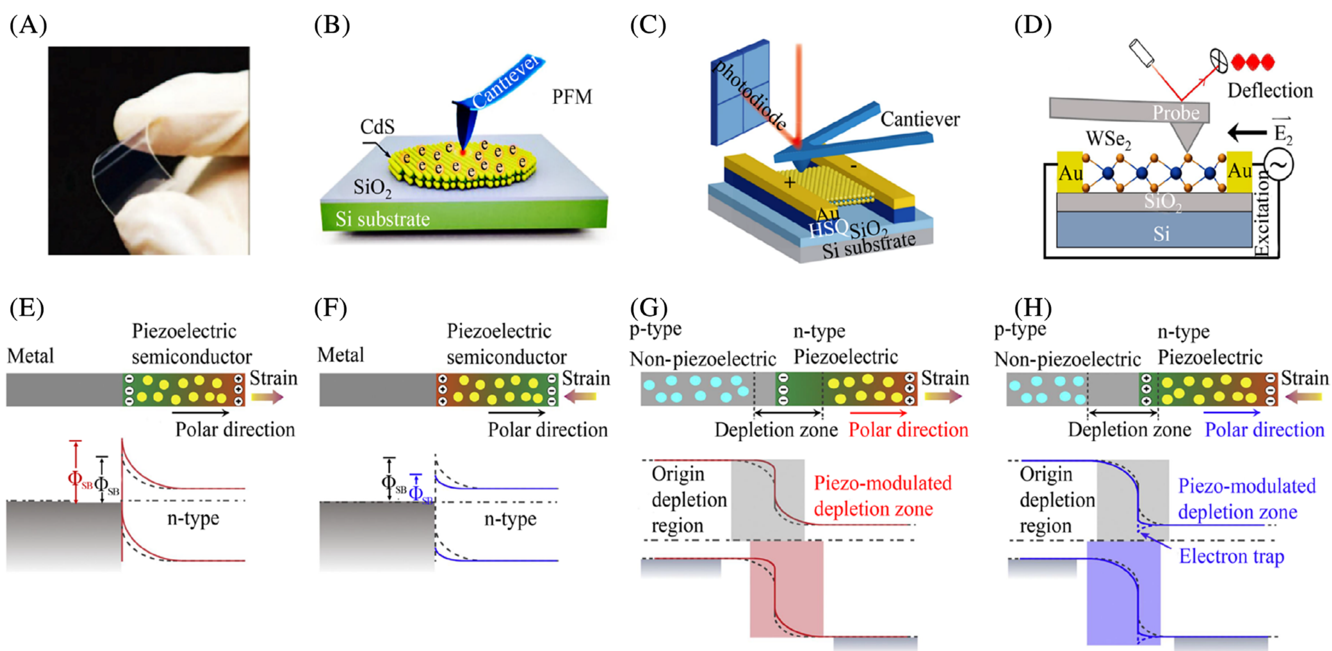

FIGURE 5 Methods for detecting piezo-response, A, Bending and releasing of flexible devices. Reproduced with permission.[31] Copyright 2014, Springer Nature. B, AFM. Reproduced with permission.[137] Copyright 2014, Springer Nature. C, PFM. Reproduced with permission.[145] Copyright 2016, American Association for the Advancement of Science. D, SPM. Reproduced with permission.[149] Copyright 2018 Elsevier Ltd. E,F, Modulated SBH in the interface between metal and n-type 2D materials, when applied the tensile strain (E) and compressive strain (F). Reproduced with permission.[44] Copyright 2018, Elsevier Ltd. G,H, Regulated energy band structure and depletion zone in p-n junction with n-type 2D materials as piezotronic materials, when applied the tensile strain (G) and compressive strain (H). Reproduced with permission.[44] Copyright 2018, Elsevier Ltd

sensors,[158–180] nanogenerators,[181–192] piezo-catalysis,[193–195] information storage,[196–199] and so on.

4.1 | Sensors

For the superiority of enhanced responsiveness of sensors combined with piezotronics, compared with those of Ohmic contact, trace sensors based on 2D piezotronic materials have been developed to enhance the sensitivity and lower the detected limitation. Such as, strain, toxic gas, pulse blood pressure, photodetector, humidity, and so on.

4.1.1 | Strain sensor

The basic principle of 2D piezotronics is to transform mechanical signal to electrical signal under the external strain. Therefore, strain sensor is the basic sensing in 2D piezotronics sensors. Zhang et al. investigated the conductivity of MoS_2 devices with AFM tip contacting at the center and near the edge of the triangular sample (Figure 6A–C).[138] When contacting at the center of MoS_2, the interaction can be equaled to compressive stress which induces negative piezo-charges in the interface, resulting in enhanced conductivity of MoS_2. While contacting near the edge of MoS_2 leads to reduced conductivity for the positive piezo-charges in the interface. The highest gauge factor of those AFM tip contacting is more than 1000 larger than those of conventional metal sensors. Then, Hu et al. found grain boundaries in monolayer MoS_2 can enhance piezotronic effect for generating polarization along both sides of the grain boundaries (Figure 6D–F).[162] Hu group also realized high spatial strain resolution of ~500 μm in 2D In_2Se_3 device, where gauge factor of the strain sensor is 237 with uniaxial strain from −0.39% to 0.39%, which is two orders of magnitude higher sensitivity than graphene-based strain sensors.[164] Another outstanding contribution is piezotronic strain-gated OR logic gates achieved by Wang group.

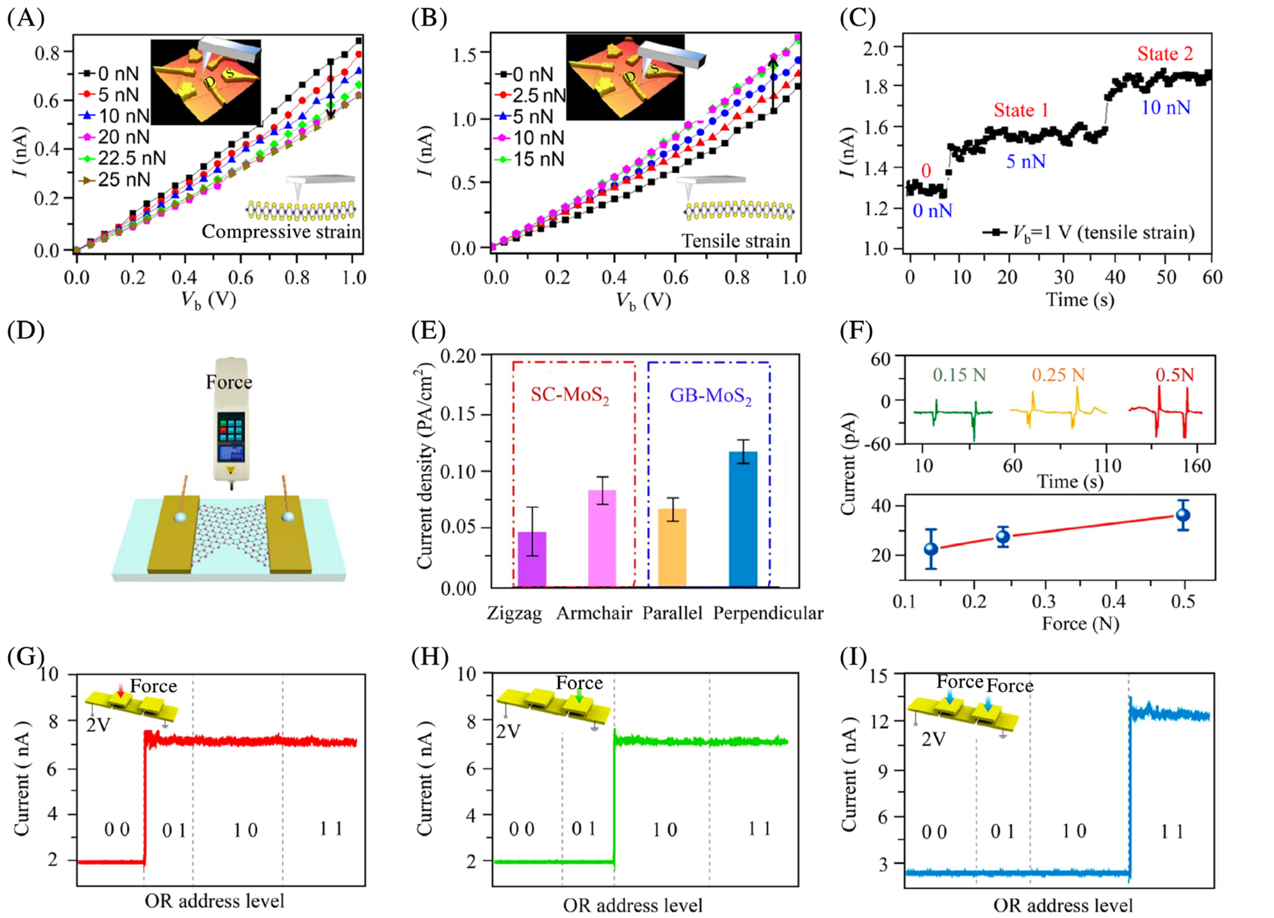

FIGURE 6 A,B, I–V_b characteristics of MoS_2 device with AFM tip contacting the center (A) and near the edge (B) of triangular film. C, Current response on different strain. Reproduced with permission.[138] Copyright 2015, Spring Nature. D, Schematic diagram of measured current with grain boundary. E, Current density of monolayer MoS_2 without and with grain boundaries. F, Output current under different strain. Reproduced with permission.[162] Copyright 2020, American Chemical Society. G–I, Strain-gated OR logic gates of ZnO piezotronics transistors. Reproduced with permission.[164] Copyright 2018, American Chemical Society

Four states, "00", "01", "10", "11" are identified by the output current in ultrathin ZnO piezotronics transistor with 2 nm channel length. "00" state is without strain and "11" state is the simultaneous stress on source and drain electrodes (Figure 6G–I).[163] Those qualitative research have pioneered, and quantitative research is needed to promote practical applications in future.

4.1.2 | Gas sensor

For the large surface area and higher sensitivity improved by piezotronics, toxic gas sensors have been researched in full swing.[160,166,167] Wang group achieved highly sensitive NO_2 sensor with monolayer MoS_2 and reduced the detected limitation to 20 parts per billion (ppb) combined with piezotronics. The sensitivity is enhanced to 671% and the response time reduced to 16 s with 0.67% tensile strain when the concentration of NO_2 is 400 ppb (Figure 7A–C).[166] Then, Xue group confirmed the higher response of NH_3 sensor by piezotronics in Au-$MoSe_2$ composites.[167] Compared with the sensor of $MoSe_2$, the Au decorated $MoSe_2$ sensor provided a Schottky contact, where electrons tend to transport to Au for higher work function. When NH_3 is absorbed to Au-$MoSe_2$ composites, the electrons transported to Au will be released to

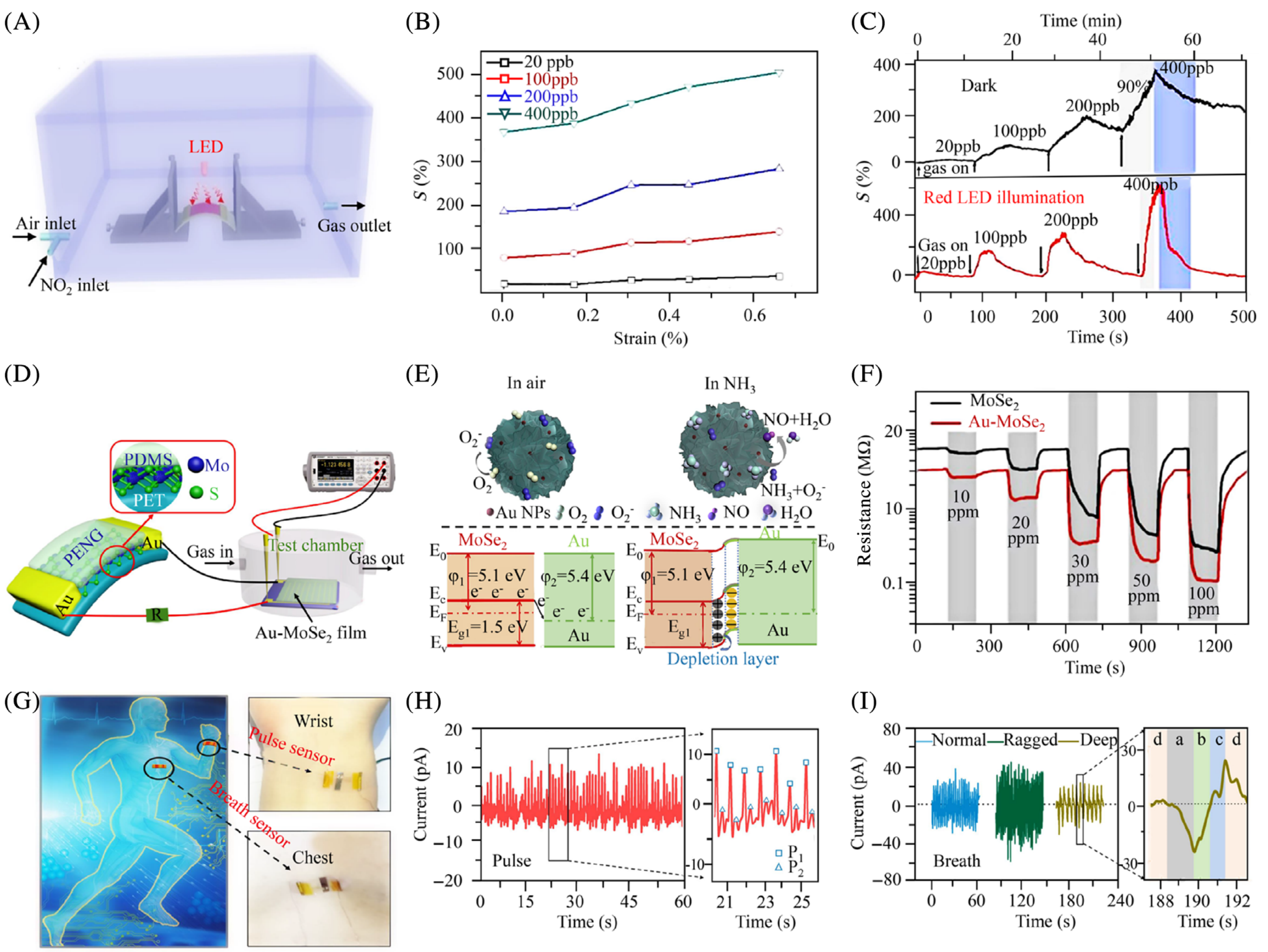

FIGURE 7 A, Schematic diagram illuminated the measurement for NO_2 sensor based on monolayer MoS_2 flexible devices. B, Dependence of gauge factor of NO_2 sensor on external strain with different NO_2 concentration. C, The response and recovery time of the NO_2 sensor without illumination and strain (I), and with 4 mW cm^{-2} red LED illumination and 0.67% tensile strain (II). Reproduced with permission.[166] Copyright 2018, Elsevier BV and Science China Press. D, Schematic illustration of self-powered NH_3 sensor driven by MoS_2-flake based piezoelectric nanogenerator. E, Schematic of NH_3 sensing mechanism and energy band structure Au-$MoSe_2$ composites. F, Dynamic resistance change of $MoSe_2$ and Au-$MoSe_2$ film sensor with different NH_3 concentration at room temperature. Reproduced with permission.[167] Copyright 2019, Elsevier Ltd. G, Schematic diagram illuminating pulse and breath sensors based on α-In_2Se_3 device. H, Pulse signals monitored by flexible α-In_2Se_3 device. I, Three breathing states monitored by flexible α-In_2Se_3 device. Reproduced with permission.[170] Copyright 2019, American Chemical Society

react with NH_3 to generate NO, which increased the output current and sensitivity (Figure 7D–F).

4.1.3 | Micro-vibration sensor

2D materials provide an important step in the development of ultra-thin flexible electronics, miniaturization, and wearable devices,[168,169] while piezotronics gives a higher sensitivity. Thus, artificial intelligence micro-vibration sensors based on 2D piezotronics were exploited significantly in recent years. Ahh et al. fabricated the MoS_2-based tactile sensor with graphene electrodes and showed perfect mechanical flexibility with the strain at 1.98%.[53] And Hu et al. reported the piezotronics based on α-In_2Se_3 flexible devices and achieved 1 order of magnitude higher piezotronic output voltage than the values of reported 2D piezotronic materials, where the output piezotronic voltage is 0.363 V for a 7-layer α-In_2Se_3 device under 1% strain.[170] The flexible devices were applied to monitor the pulse and breath signals (Figure 7G–I). The monitored pulsed signal gives two peaks obviously, responding to left ventricular ejected blood wave and reflected wave from the lower body. Besides, three types of breathing states were also monitored, corresponding to normal, ragged, and deep states, respectively. For all the cases, the output signals suggest the micro-vibration sensor based on 2D piezotronics has a good responsivity, while the temporal and spatial resolutions should be considered to further sensing.

4.1.4 | Photodetector

Piezo-potential promotes separation and transport of photogenerated electrons and holes and increases the output current, causing the enhanced photo-response and developed piezophototronics of 2D materials.[171–177] Those piezophototronic sensors can be divided into two types of contact: metal and 2D materials, and p-n junctions. For the contact of metal and 2D materials, MoS_2,[22,171,178] WSe_2,[172] α-In_2Se_3,[173] γ-InSe,[174] and $In_{1-x}Sn_xSe$,[175] were investigated widely. It is interesting that by repairing the defect in MoS_2 flexible phototransistor, a prominent piezophototronic sensor was realized, where 5.6-fold enhancement of responsivity is achieved under a 0.42% tensile strain (Figure 8A–C).[171] For the p-n junction, homogeneous and heterogeneous p-n junction were also developed (Figure 8D–F).[176] MoS_2 homogeneous p-n junction was realized by Wang group.[177] The enhancement of photoresponsivity and detectivity under 0.51% strain gives 619% and 319% compared with those without external strain. Heterogeneous p-n flexible photodiode was achieved by Li group with vertically stacking multilayer p-WSe_2 and monolayer n-MoS_2.[176] The optimized photoresponsivity increases by 86% under −0.62% strain along armchair direction of MoS_2.[177]

4.1.5 | Humidity sensor

Humidity detection has been realized in MoS_2/metal junction.[115,170] When H_2O is absorbed to monolayer MoS_2, electrons in MoS_2 are captured by H_2O molecular, resulting in reduced carrier concentration and output current. While applied the external strain to the flexible device, the piezo potential is generated along zigzag direction, which modulating SBH of MoS_2/metal interface and output current. The maximum current variation could reach 2048% with the humidity changing from 63% to 5% under 0.61% tensile strain (Figure 8G–I).[178] However, the chemical reaction between absorbed H_2O and MoS_2 will degrade 2D MoS_2 gradually, therefore, the stability and durability should be deliberated for humidity sensor in future.

4.2 | Nanogenerator

Energy harvesting based on 2D piezotronics provides a breakthrough of flexible self-powered systems for the atomic layer thickness, excellent mechanical performance, and piezotronic properties of 2D materials.[181–184] When applied the tensile or compressive strain in 2D flexible devices, piezo-potential is created in the interface of 2D materials and metal electrodes, where electrons and holes in 2D materials are attracted to opposite polarity piezo-potential and current is produced in the external circuits.[184] When the alternating strain is applied, the alternating current and voltage are generated.[185] Thus, nanogenerator, converting mechanical energy into electrical energy, is established. Wu group first reported the 2D nanogenerator based on MoS_2 with odd number of atomic layers and achieved 5.08% conversion efficiency of mechanical to electrical energy from monolayer MoS_2 nanogenerator (Figure 9A–C).[31] The piezotronic output from monolayer MoS_2 nanogenerator is directly connected to the crystal orientation for different piezoelectric coefficients along zigzag and armchair directions.[31,143] At the same time, MoS_2 nanogenerators in series or in parallel showed consistent enhancements in output voltages or currents, suggesting potential practical application for powering nanodevices.

Since then, 2D nanogenerators based on various 2D materials have been researched passionately, such as $MoSe_2$,[47] α-In_2Se_3,[49] BP,[55] hollow 2D MoS_2 shells,[185] BN,[186] ZnO,[187,188] bilayer WSe_2,[191] multi-pores MoS_2,[192] and so on. The bilayer WSe_2 nanogenerator indicates that stacking direction of TMDCs with even number of atomic

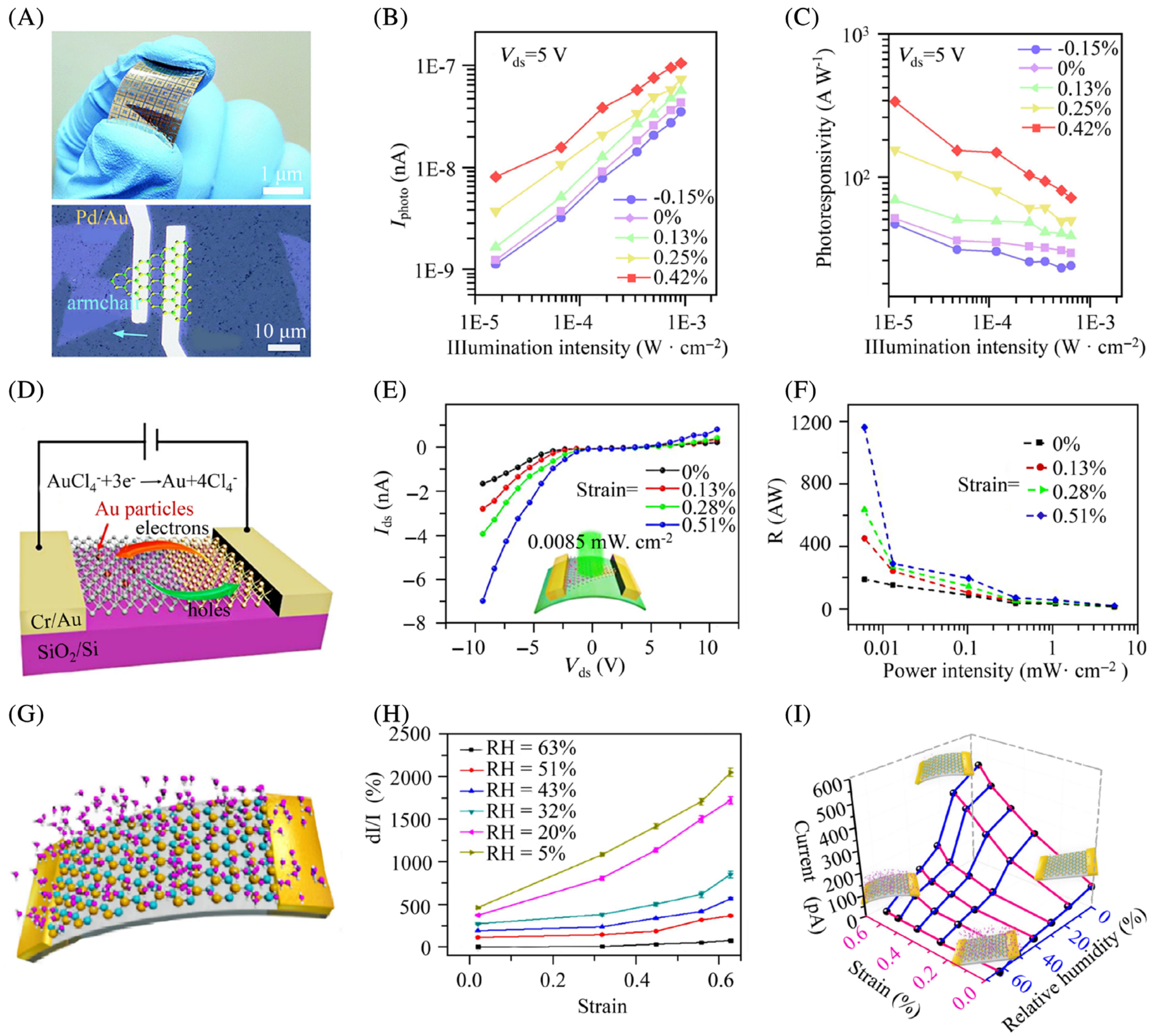

FIGURE 8 A, Optical image of the flexible piezophototronic detector fabricated with monolayer MoS_2 on the PET substrate. B,C, Strain dependence of photocurrent (B) and photoresponsivity (C) on different illumination intensities. Reproduced with permission.[171] Copyright 2018, American Chemical Society. D, Schematic diagram of monolayer MoS_2 homogenous p-n junction. E, I_{ds}–V_{ds} characteristics of MoS_2 homogenous p-n junction with different tensile strains. F, Photoresponsivity of MoS_2 homogenous p-n junction under different strains and excited intensities. Reproduced with permission.[176] Copyright 2018, IOP Publishing Ltd. G, Schematic diagram of MoS_2/metal flexible device for humidity detection. H, Dependence of changed relative current on external strain with different relative humidity (RH). I, Dependence of current response on various strains and RH at a bias voltage of 10 V. Reproduced with permission.[178] Copyright 2018, American Chemical Society

layers determines symmetry and piezotronic performance (Figure 9D–F).[191] Another significant work is nano-powered generator by monolayer MoS_2 nanopores, designed by Radenovic group (Figure 9G–I).[192] Two liquids with different concentrations are separated by MoS_2 nanopores, therefore, a chemical potential gradient was formed so that the ions could travel across the nanopore spontaneously. For the surface charges around the nanopores, passing ions will be selected according to charge polarity, resulting in a net osmotic current. The output voltage and current of this nanogenerator have been successfully powered a MoS_2 transistor. All those pioneering works have laid the foundation for practical applications of nanogenerators, the integrated and wearable nanogenerators need be scheduled in future.

4.3 | Piezo-catalysis

Photocatalytic water splitting and degradation of organic pollutants are considered the most promising solution to energy crisis and environmental pollution.

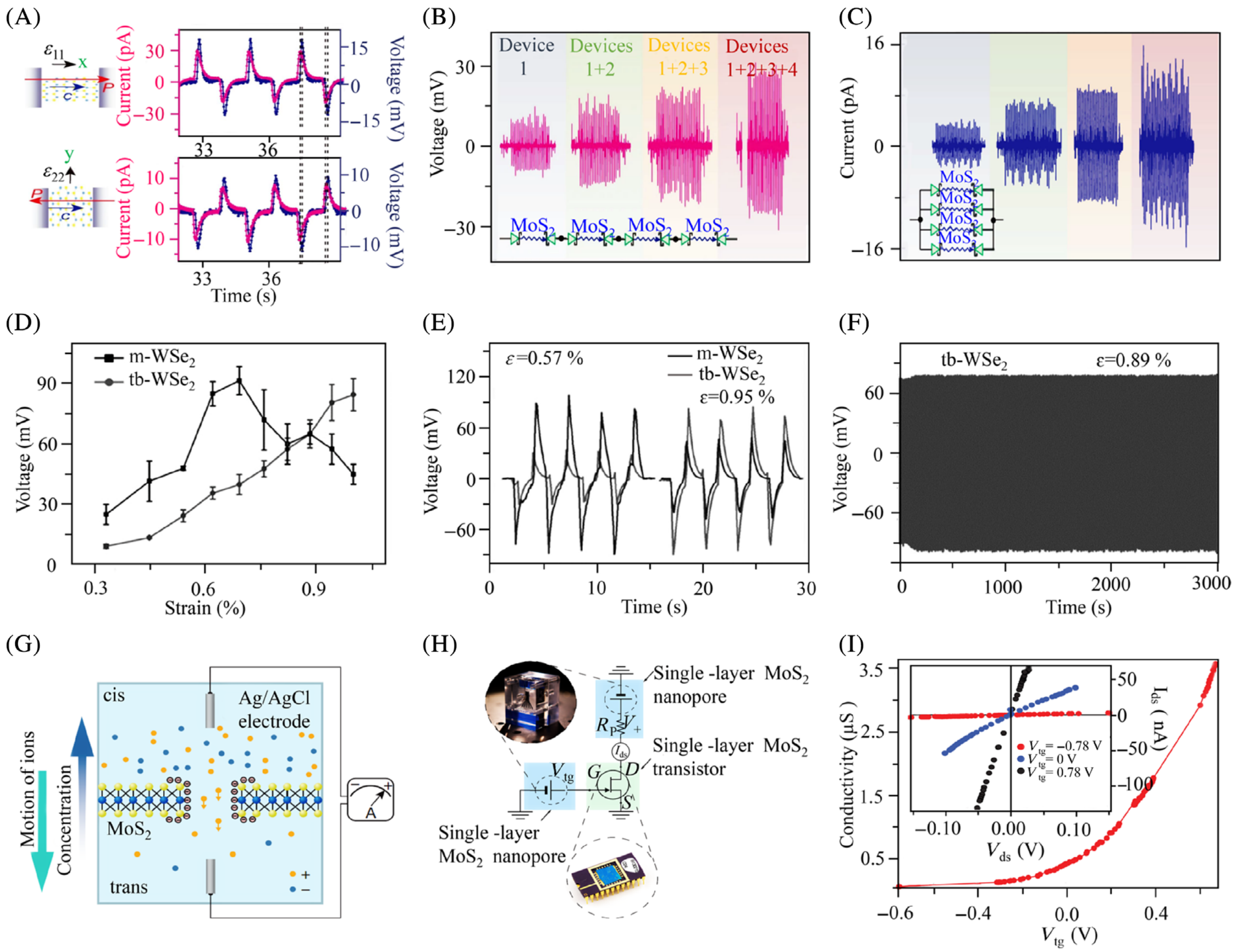

FIGURE 9 A, Output current along armchair and zigzag directions of monolayer MoS_2 nanogenerators. B, Output voltage of four monolayer MoS_2 nanogenerators in parallel. C, Output current of four monolayer MoS_2 nanogenerators in series. Reproduced with permission.[31] Copyright 2014, Springer Nature. D, Dependence of output voltage of monolayer WSe_2 (m-WSe_2) and transferred bilayer WSe_2 (tb-WSe_2) nanogenerators on external strain. E, Output voltage of m-WSe_2 and tb-WSe_2 nanogenerators with strain at 0.57% and 0.95%. F, The durability test of m-WSe_2 and tb-WSe_2 nanogenerators with the strain at 0.89%. Reproduced with permission.[191] Copyright 2017, Wiley-VCH. G, Schematic of MoS_2 nanopores as nanogenerators. H, Schematic diagram of the self-powered MoS_2 transistor, where the current between drain (D) and source (S) is supplied by a MoS_2 nanopore nanogenerators and the gate (G) source is supported by the other MoS_2 nanopore nanogenerators. I, Transfer curve of the self-powered MoS_2 transistor. Reproduced with permission.[192] Copyright 2016, Springer Nature

The suitable bandgap of 2D materials for absorbing visible light from sunlight establishes the photocatalytic foundation, and piezotronics enhances photocatalytic performance. MoS_2, WSe_2, CdS, and WS_2 have been applied to catalytic water splitting or degrade organic pollutants with the application of ultrasonic vibration.[193–195] The piezopotential induced by ultrasonic vibration encourages the separation of holes and electrons in 2D materials, which reacted with water and dissolved O_2 to generate •OH and •O_2^- radicals to degrade pollutants (Figure 10D–F).[195] However, the enhanced performance by piezotronics calculated in articles was also contained the separation of various radicals and degraded small molecules promoted by ultrasonic vibration natively, which increase the photocatalytic behaviors simultaneously. And the significant lattice bending of multilayer nanosheets from MoS_2, WS_2, and WSe_2 should be also considered, which inducing piezopotential initially and might influence the piezo-catalytic mechanism and performance simultaneously.

4.4 | Information storage

Information storage is the basic engineering for artificial intelligence, where memristors are considered to be the perfect candidates for nonvolatile memories and artificial

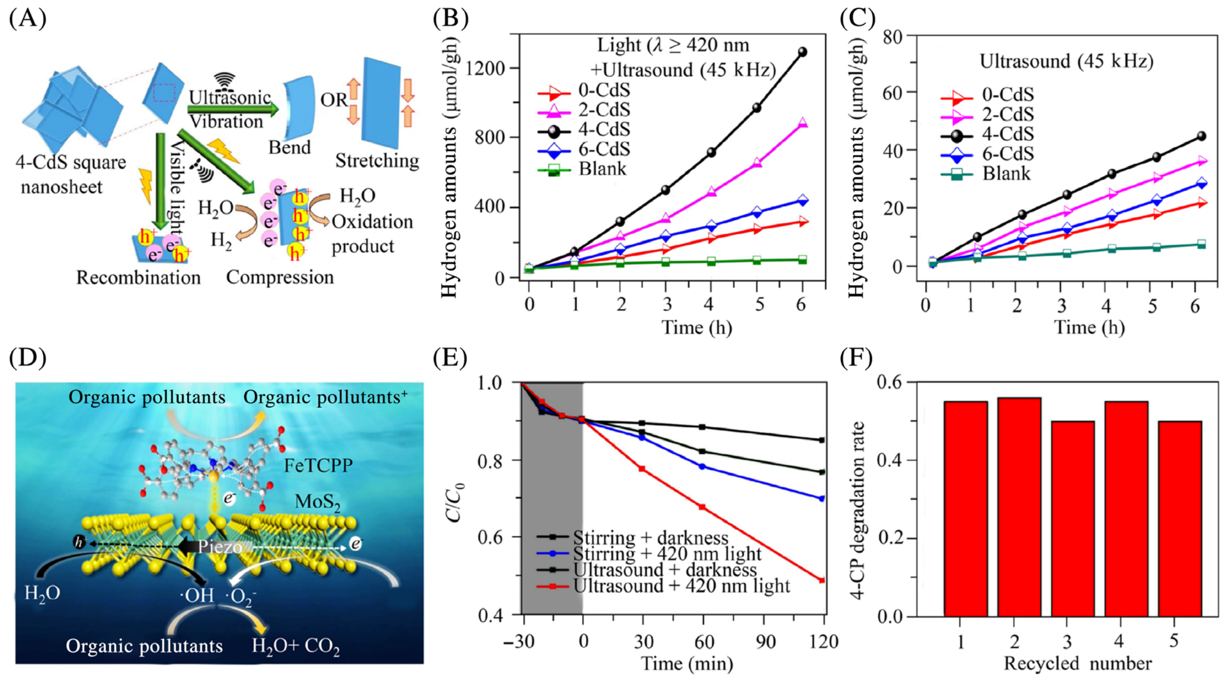

FIGURE 10 A, Schematic diagram illustrated photo-/piezo-catalytic mechanism of CdS nanosheet. B,C, Time depended catalytic performance with (B) and without (C) light. Reproduced with permission.[193] Copyright 2020, Springer Nature. D, Schematic showing the piezo-/photo-catalytic mechanism of FETCP/MoS_2 nanosheet. E, Catalytic degradation of FETCP/MoS_2 nanosheet with different condition. F, Cycling degradation tests of FETCP/MoS_2 nanosheet. Reproduced with permission.[195] Copyright 2019, Elsevier BV

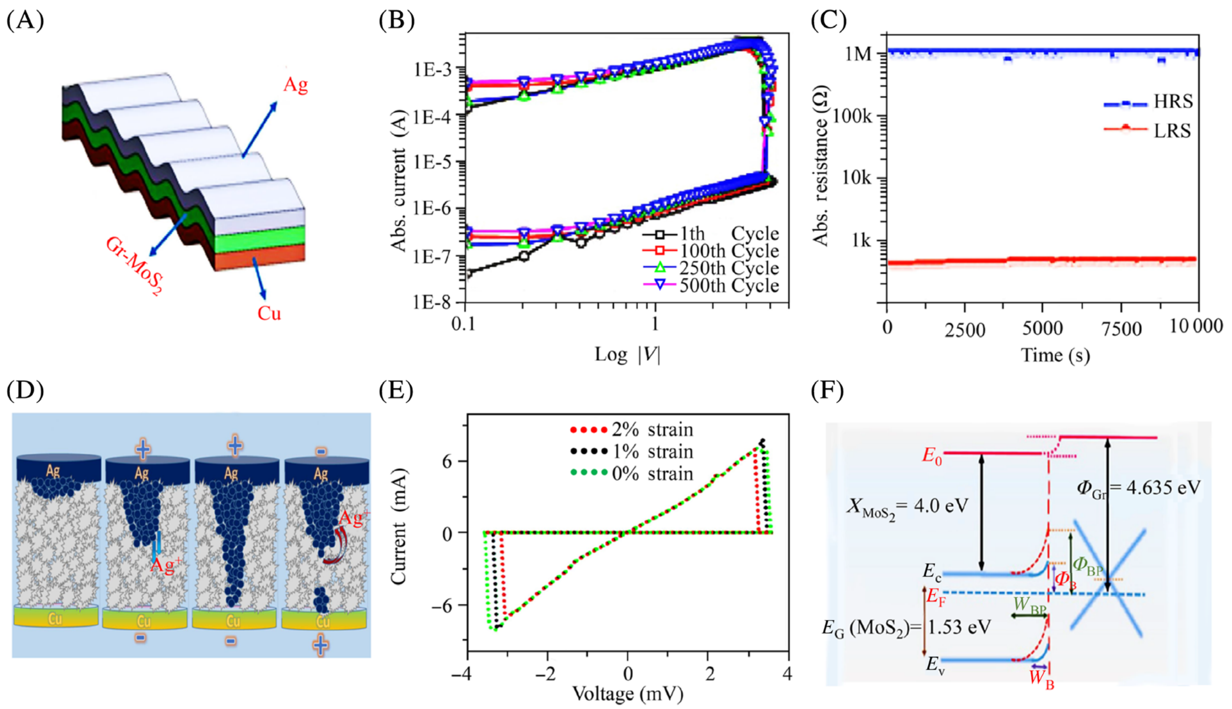

FIGURE 11 A, Schematic of graphene/MoS_2 flexible device. B,C, Repeatability (B) and retention (C) of graphene/MoS_2 flexible device. D, Schematic illuminates resistive switching mechanism. E, *I–V* curves of graphene/MoS_2 flexible device under different strain. F, Energy band diagram with piezotronic effect of graphene/MoS_2 flexible device. Reproduced with permission.[196] Copyright 2019, American Chemical Society

intelligence.[196–199] Badhulika et al. fabricated piezotronic memristor based on graphene/MoS_2 2D nanohybrid, where graphene improves the mobility for conductivity.[196] The graphene/MoS_2 memory shows excellent stability with resistive switching 500 cycles and endurance with data retention of 10^4 s under 10^4 On/Off ratio (Figure 11). Ag ions from the top Ag electrode penetrate to the Cu electrodes gradually by increasing the voltage between Ag and Cu electrodes, leading to the "On" state. When applied the external strain, the negative potential is created in the interface between graphene and MoS_2, causing reduced SBH, enhanced voltage distribution and electric field intensity between MoS_2 and Ag electrode. Thus, the drift velocity of Ag ions increases and the voltage for "On" state is reduced with increasing the external strain.

Information storage is a new direction for 2D piezotronics. Careful design and lots of attention should be paid to exploit the performance vigorously. For example, reduced the "On" state voltage by reasonable designing the thickness and quality of MoS_2. Designing arrayed devices with different "On" state voltage are applied to store various information with avoiding serial interference.

5 | CONCLUSIONS AND PROSPECT

In this review, we present the 2D piezotronic materials from inorganic to organic crystals with the original or modulated centrosymmetric structure. Four kinds of experimental measurement methods and mechanism of 2D piezotronics are described, containing bending and releasing of flexible devices, AFM, PFM, and SPM. Various applications were also exploited to improve the sensitivity, limitation, resolution, and durability, such as different sensors, nanogenerators, piezo-catalysis, and information storage. Although the preliminary work has laid the foundation for future research, challenges are always existed in 2D piezotronics. Efforts might be engaged as follows:

1. Excepting the piezo-potential induced by the external strain, the electric band structure of 2D materials is also sensitive to pressure engineering,[200,201] which influences the transport of electrons significantly. The output performance of 2D piezotronics devices is decided by SBH between 2D materials and electrodes,[202] determined by the energy of conduction band minimum or valence band maximum for n-type or p-type 2D materials, respectively. However, the external strain also modulates bandgap and energy band extremum, further, the conductivity type and output currents.[203–205] For example, the bandgap of monolayer MoS_2 will be decreased from 1.883 to 1.690 eV under 1.49% compressive strain.[203] The valence band maximum of monolayer MoS_2 shifts from K point to Γ point when applying compressive strain, while conduction band minimum shifts from K to the point between K and Γ points.[204] Besides, the conductivity type of monolayer TMDC could change from semiconductor to metal under 11% external strain.[205] The changed bandgap and shifted extreme point in reciprocal space have a great influence on output voltage and currents, which might be calculated in present experiments. Thus, modulated output voltage and current in 2D piezotronics should be considered the energy band engineering simultaneously.
2. The various applications are the preliminary, qualitative, quantitative research, and comparative exploration in vertical and horizontal need be launched. For example, for the piezo-catalysis, the types and concentration of defects in 2D materials should be considered. For the various types of sensors, statistical results should be performed for the inhomogeneous crystal structure and local designed devices in single sheet of 2D materials.
3. The separation and transport of electrons and holes in different defects by piezotronics need to be calculated and confirmed by experiments exhaustively. Defects are the intrinsic properties in 2D materials, which affect the carrier transport, electronic and optical properties significantly.[206] The well-known defects are cationic or anionic vacancies, dislocations, and grain boundaries, and so on, which are confirmed by first-principles calculations and observed by high-angle annular dark field scanning transmission electron microscopy (HAADF-STEM).[207–209] The concentration, distribution, and orientation of point defects influence the separation and transport of carrier, resulting in anisotropic electrical performance with the same type of defect and different conductivities along the same crystal orientation with different types of defects.[210–212] Meanwhile, the external strain can change the distribution and types of defects.[213–216] First, the tensile strain could lower the activation energy of vacancy migration and induce the migration of vacancies,[213,214] leading to the redistribution of vacancies, furtherly, changing the point defects to dislocation. Second, the external strain favors the generation of vacancies in 2D materials,[215] resulting in the increasing concentration of vacancies. Third, the orientation of line defects also depends on the mechanical strain,[216] which might rotate the orientation of dislocation. Therefore, external strain could alter the concentration, distribution, and types of defects, which might influence the separation and transport of carrier and electrical performance. However, the

changed electrical performance induced by external strain might be calculated in present piezotronics experiments. Thus, the carrier separation and transport related to defects in piezotronics need to be calculated and confirmed by experiments.

4. For the purpose of final practical application, arrayed flexible devices with 2D piezotronics should be exploited with avoiding serial interference. The refraction, diffraction, boundary reflection, and photon scattering in 2D materials and arrayed devices might cause serial interference and influence the resolution of flexible devices during piezo-phototronics experiments.[217,218] At the same time, the carrier generation and diffusion might lead to electrical serial interference in piezotronics, which is connected to the size, spacing, and distribution of single device, buffer layer thickness, and epitaxial layer thickness of arrayed devices.[219,220] In order to avoid the serial interference, independent electrodes for any single device in arrayed devices are needed, which are difficult for design and fabrication of arrayed devices. Thus, reasonable design of flexible arrayed devices is necessary to reduce the serial interference.
5. The growth of 2D materials needs further development. Large area 2D materials and heterojunction materials with the order of magnitude from centimeter to meter are urgently needed. And the 2D piezotronics based on heterojunction should be explored in full swing.
6. The experimental method of bending and releasing of flexible devices for 2D piezotronics should be paid much attention because the method is closer to practical applications. And the measured method of 2D piezotronics need to be expanded furtherly.

ACKNOWLEDGMENTS

The authors thank the support of National Natural Science Foundation of China (Nos. 11704081, U20A20166, 61675027, 61805015, and 61804011), National Key R&D project from Minister of Science and Technology, China (2016YFA0202703), Natural Science Foundation of Beijing Municipality (Z180011), Natural Science Foundation of Guangxi Province (Nos. 2020GXNSFAA297182 and 2017GXNSFBA198229), Shenzhen Science and Technology Program (Grant No. KQTD20170810105439418), and the Fundamental Research Funds for the Central Universities.

CONFLICT OF INTEREST

The authors declare no conflict of interest.

ORCID

Caofeng Pan https://orcid.org/0000-0001-6327-9692

REFERENCES

1. Wang ZL, Song JH. Piezoelectric nanogenerators based on zinc oxide nanowire arrays. *Science*. 2006;312:242-246.
2. Wang ZL. Nanopiezotronics. *Adv Mater*. 2007;19:889-892.
3. Yang Q, Wang W, Xu S, Wang ZL. Enhancing light emission of ZnO microwire-based diodes by piezo-phototronic effect. *Nano Lett*. 2011;11:4012-4017.
4. Bao RR, Tao J, Pan CF, Wang ZL. Piezo-phototronic effect in nano-sensors. *Small Sci*. 2021;1:2000060.
5. Dai Z, Liu L, Zhang Z. Strain engineering of 2D materials: issues and opportunities at the interface. *Adv Mater*. 2019;31:e1805417.
6. Deng S, Sumant AV, Berry V. Strain engineering in two-dimensional nanomaterials beyond graphene. *Nano Today*. 2018;22:14-35.
7. Guo J, Zhao J, Huang D, et al. Two-dimensional tellurium-polymer membrane for ultrafast photonics. *Nanoscale*. 2019;11:6235-6242.
8. Wang QH, Kalantar-Zadeh K, Kis A, Coleman JN, Strano MS. Electronics and optoelectronics of two-dimensional transition metal dichalcogenides. *Nat Nanotechnol*. 2012;7:699-712.
9. Liu Y, Bao R, Tao J, Li J, Dong M, Pan C. Recent progress in tactile sensors and their applications in intelligent systems. *Sci Bull*. 2020;65:70-88.
10. Pan C, Dong L, Zhu G, et al. High-resolution electroluminescent imaging of pressure distribution using a piezoelectric nanowire LED array. *Nat Photon*. 2013;7:752-758.
11. Yu R, Niu S, Pan C, Wang ZL. Piezotronic effect enhanced performance of Schottky-contacted optical, gas, chemical and biological nanosensors. *Nano Energy*. 2015;14:312-319.
12. Zhang H, Peng D, Wang W, Dong L, Pan C. Mechanically induced light emission and infrared-laser-induced upconversion in the Er-doped CaZnOS multifunctional piezoelectric semiconductor for optical pressure and temperature sensing. *J Phys Chem C*. 2015;119:28136-28142.
13. Brotons-Gisbert M, Proux R, Picard R, et al. Out-of-plane orientation of luminescent excitons in two-dimensional indium selenide. *Nat Commun*. 2019;10:3913.
14. Ma W, Lu J, Yang Z, et al. Crystal-orientation-related dynamic tuning of the lasing spectra of CdS nanobelts by piezoelectric polarization. *ACS Nano*. 2019;13:5049-5057.
15. Lin H, Xu ZQ, Cao G, et al. Diffraction-limited imaging with monolayer 2D material-based ultrathin flat lenses. *Light Sci Appl*. 2020;9:137.
16. Sun Z, Martinez A, Wang F. Optical modulators with 2D layered materials. *Nat Photon*. 2016;10:227-238.
17. Huang Z, Han W, Tang H, et al. Photoelectrochemical-type sunlight photodetector based on MoS_2/graphene heterostructure. *2D Mater*. 2015;2:035011.
18. Lee HS, Min SW, Chang YG, et al. MoS_2 nanosheet phototransistors with thickness-modulated optical energy gap. *Nano Lett*. 2012;12:3695-3700.
19. Li F, Qi J, Xu M, et al. Layer dependence and light tuning surface potential of 2D MoS_2 on various substrates. *Small*. 2017;13:1603103.
20. Wang J, Han J, Chen X, Wang X. Design strategies for two-dimensional material photodetectors to enhance device performance. *InfoMat*. 2019;1:33-53.

21. Withers F, Pozo-Zamudio OD, Mishchenko A, et al. Light-emitting diodes by band-structure engineering in van der Waals heterostructures. *Nat Mater*. 2015;14:301-306.
22. Wu W, Wang L, Yu R, et al. Piezophototronic effect in single-atomic-layer MoS_2 for strain-gated flexible optoelectronics. *Adv Mater*. 2016;28:8463-8468.
23. Qiao S, Cong R, Liu J, et al. A vertically layered MoS_2/Si heterojunction for an ultrahigh and ultrafast photoresponse photodetector. *J Phys Chem C*. 2018;6:3233-3239.
24. Wu JP, Wang L, Zhang LY. Rapid and nondestructive layer number identification of two-dimensional layered transition metal dichalcogenides. *Rare Metals*. 2017;36:698-703.
25. Novoselov KS, Geim AK, Morozov SV, et al. Electric field effect in atomically thin carbon films. *Science*. 2004;306: 666-669.
26. Chang HY, Yogeesh MN, Ghosh R, et al. Large-area monolayer MoS_2 for flexible low-power RF nanoelectronics in the GHz regime. *Adv Mater*. 2016;28:1818-1823.
27. Larentis S, Fallahazad B, Tutuc E. Field-effect transistors and intrinsic mobility in ultra-thin $MoSe_2$ layers. *Appl Phys Lett*. 2012;101:223104.
28. Liu W, Kang J, Sarkar D, Khatami Y, Jena D, Banerjee K. Role of metal contacts in designing high-performance monolayer n-type WSe_2 field effect transistors. *Nano Lett*. 2013;13:1983-1990.
29. Neri I, López-Suárez M. Electronic transport modulation on suspended few-layer MoS_2 under strain. *Phys Rev B*. 2018;95: 241408.
30. Radisavljevic B, Radenovic A, Brivio J, Giacometti V, Kis A. Single-layer MoS_2 transistors. *Nat Nanotechnol*. 2011;6: 147-150.
31. Wu W, Wang L, Li Y, et al. Piezoelectricity of single-atomic-layer MoS_2 for energy conversion and piezotronics. *Nature*. 2014;514:470-474.
32. Yoon Y, Ganapathi K, Salahuddin S. How good can monolayer MoS_2 transistors be? *Nano Lett*. 2011;11:3768-3773.
33. Zhao J, Wei Z, Zhang Q, et al. Static and dynamic piezopotential modulation in piezo-electret gated MoS_2 field-effect transistor. *ACS Nano*. 2019;13:582-590.
34. Gargiani P, Cuadrado R, Vasili HB, Pruneda M, Valvidares M. Graphene-based synthetic antiferromagnets and ferrimagnets. *Nat Commun*. 2017;8:699.
35. Gong C, Zhang X. Two-dimensional magnetic crystals and emergent heterostructure devices. *Science*. 2019;363:eaav4450.
36. Dankert A, Langouche L, Kamalakar MV, Dash SP. High-performance molybdenum disulfide field-effect transistors with spin tunnel contacts. *ACS Nano*. 2014;8:476-482.
37. Liu X, Song C, Wu Z, Wang J, Pan J, Li C. Bandgap opening and magnetic anisotropy switching by uniaxial strain in graphene/CrI_3 heterojunction. *J Phys D Appl Phys*. 2020;53:385002.
38. Yang Q, Kou L, Hu X, et al. Strain robust spin gapless semiconductors/half-metals in transition metal embedded $MoSe_2$ monolayer. *J Phys Condens Matter*. 2020;32:365305.
39. Cortie DL, Causer GL, Rule KC, Friyzsche H, Kreuzpaintner W, Klose F. Two-dimensional magnets: forgotten history and recent progress towards spintronic applications. *Adv Funct Mater*. 2020; 30:1901414.
40. Guo Y, Wang B, Zhang X, Yuan S, Ma L, Wang J. Magnetic two-dimensional layered crystals meet with ferromagnetic semiconductors. *InfoMat*. 2020;2:639-655.
41. Zuo SL, Chen P, Pan CF. Mechanism of magnetic field-modulated luminescence from lanthanide ions in inorganic crystal: a review. *Rare Metals*. 2020;39:1113-1126.
42. Huang X, Liu W, Zhang A, Zhang Y, Wang Z. Ballistic transport in single-layer MoS_2 piezotronic transistors. *Nano Res*. 2015;9:282-290.
43. Jiang H, Zheng L, Liu Z, Wang X. Two-dimensional materials: from mechanical properties to flexible mechanical sensors. *InfoMat*. 2020;2:1077-1094.
44. Lin P, Pan C, Wang ZL. Two-dimensional nanomaterials for novel piezotronics and piezophototronics. *Mater Today Nano*. 2018;4:17-31.
45. Hu G, Zhou R, Yu R, Dong L, Pan C, Wang ZL. Piezotronic effect enhanced Schottky-contact ZnO micro/nanowire humidity sensors. *Nano Res*. 2014;7:1083-1091.
46. Rawat A, Mohanta MK, Jena N, Dimple, Ahammed R, De Sarkar A. Nanoscale interfaces of Janus monolayers of transition metal dichalcogenides for 2D photovoltaic and piezoelectric applications. *J Phys Chem C*. 2020;124:10385-10397.
47. Li P, Zhang Z. Self-powered 2D material-based PH sensor and photodetector driven by monolayer $MoSe_2$ piezoelectric nanogenerator. *ACS Appl Mater Interfaces*. 2020;12:58132-58139.
48. Yuan S, Io WF, Mao J, Chen Y, Luo X, Hao J. Enhanced piezoelectric response of layered In_2Se_3/MoS_2 nanosheet-based van der Waals heterostructures. *ACS Appl Nano Mater*. 2020; 3:11979-11986.
49. Xue F, Zhang J, Hu W, et al. Multidirection piezoelectricity in mono- and multilayered hexagonal α-In_2Se_3. *ACS Nano*. 2018; 12:4976-4983.
50. Han X, Du W, Yu R, Pan C, Wang ZL. Piezo-phototronic enhanced UV sensing based on a nanowire photodetector array. *Adv Mater*. 2015;27:7963-7969.
51. Chen M, Zhao B, Hu G, et al. Piezo-phototronic effect modulated deep UV photodetector based on ZnO-Ga_2O_3 heterojunction microwire. *Adv Funct Mater*. 2018;28:1706379.
52. Jiang C, Li Q, Huang J, Bi S, Ji R, Guo Q. Single-layer MoS_2 mechanical resonant piezo-sensors with high mass sensitivity. *ACS Appl Mater Interfaces*. 2020;12:41991-41998.
53. Park M, Park YJ, Chen X, Park YK, Kim MS, Ahn JH. MoS_2-based tactile sensor for electronic skin applications. *Adv Mater*. 2016;28:2556-2562.
54. Chen L, Xue F, Li X, et al. Strain-gated field effect transistor of a MoS_2-ZnO 2D-1D hybrid structure. *ACS Nano*. 2016;10: 1546-1551.
55. Ma W, Lu J, Wan B, et al. Piezoelectricity in multilayer black phosphorus for piezotronics and nanogenerators. *Adv Mater*. 2020;32:e1905795.
56. Li Z, Zhang T, Fan F, Gao F, Ji H, Yang L. Piezoelectric materials as Sonodynamic sensitizers to safely ablate tumors: a case study using black phosphorus. *J Phys Chem Lett*. 2020;11:1228-1238.
57. Huang L, Li Y, Wei Z, Li J. Strain induced piezoelectric effect in black phosphorus and MoS_2 van der Waals heterostructure. *Sci Rep*. 2015;5:16448.
58. Wan B, Guo S, Sun J, et al. Investigating the interlayer electron transport and its influence on the whole electric properties of black phosphorus. *Sci Bull*. 2019;64:254-260.
59. Buscema M, Groenendijk DJ, Steele GA, Zant HSJ, Castellanos-Gomez A. Photovoltaic effect in few-layer black

phosphorus PN junctions defined by local electrostatic gating. *Nat Commun*. 2014;5:4651.

60. Noor-A-Alam M, Kim HJ, Shin YH. Dipolar polarization and piezoelectricity of a hexagonal boron nitride sheet decorated with hydrogen and fluorine. *Phys Chem Chem Phys*. 2014;16: 6575-6582.
61. Ares P, Cea T, Holwill M, et al. Piezoelectricity in monolayer hexagonal boron nitride. *Adv Mater*. 2019;32:1905504.
62. Michel KH, Cakir D, Sevik C, Peeters FM. Piezoelectricity in two-dimensional materials: comparative study between lattice dynamics and ab initio calculations. *Phy Rev B*. 2017;95:125415.
63. Blonsky MN, Zhuang HL, Singh AK, Hennig RG. Ab initio prediction of piezoelectricity in two-dimensional materials. *ACS Nano*. 2015;9:9885-9891.
64. Duerloo KAN, Ong MT, Reed EJ. Intrinsic piezoelectricity in two-dimensional materials. *J Phys Chem Lett*. 2012;3:2871-2876.
65. Alyörük MM, Aierken Y, Çakır D, Peeters FM, Sevik C. Promising piezoelectric performance of single layer transition-metal dichalcogenides and dioxides. *J Phys Chem C*. 2015;119: 23231-23237.
66. Kang S, Kim S, Jeon S, et al. Atomic-scale symmetry breaking for out-of-plane piezoelectricity in two-dimensional transition metal dichalcogenides. *Nano Energy*. 2019;58:57-62.
67. Lu AY, Zhu H, Xiao J, et al. Janus monolayers of transition metal dichalcogenides. *Nat Nanotechnol*. 2017;12:744-749.
68. Reed EJ. Now in two dimensions. *Nat Nanotechnol*. 2015;10: 106-107.
69. Sohn A, Choi S, Han SA, et al. Temperature-dependent piezotronic effect of MoS_2 monolayer. *Nano Energy*. 2019;58: 811-816.
70. Hinchet R, Khan U, Falconi C, Kim SW. Piezoelectric properties in two-dimensional materials: simulations and experiments. *Mater Today*. 2018;21:611-630.
71. Dong L, Lou J, Shenoy VB. Large in-plane and vertical piezoelectricity in janus transition metal dichalchogenides. *ACS Nano*. 2017;11:8242-8248.
72. Sevik C, Çakır D, Gülseren O, Peeters FM. Peculiar piezoelectric properties of soft two-dimensional materials. *J Phys Chem C*. 2016;120:13948-13953.
73. Liu JB, Hu JY, Liu C, Tan YM, Peng X, Zhang Y. Mechanically exfoliated MoS_2 nanosheets decorated with SnS_2 nanoparticles for high-stability gas sensors at room temperature. *Rare Metals*. 2020;40:1536-1544.
74. Tu ZC, Hu X. Elasticity and piezoelectricity of zinc oxide crystals, single layers, and possible single-walled nanotubes. *Phys Rev B*. 2006;74:035434.
75. Wang L, Liu S, Zhang Z, et al. 2D piezotronics in atomically thin zinc oxide sheets: interfacing gating and channel width gating. *Nano Energy*. 2019;60:724-733.
76. Heyd J, Peralta JE, Scuseria GE, Martin RL. Energy band gaps and lattice parameters evaluated with the Heyd–Scuseria–Ernzerhof screened hybrid functional. *J Chem Phys*. 2005;123: 174101.
77. Zheng H, Li X, Chen N, et al. Monolayer II–VI semiconductors: a first-principles prediction. *Phys Rev B*. 2015;92:115307.
78. Zhuang H, Hennig R. Computational identification of single-layer CdO for electronic and optical applications. *Appl Phys Lett*. 2013;103:212102.
79. Alyörük MM. Piezoelectric properties of monolayer II-VI group oxides by first-principles calculations. *Phys Status Solidi B*. 2016;253:2534-2539.
80. Hess P. Thickness of elemental and binary single atomic monolayers. *Nanoscale Horiz*. 2020;5:385-399.
81. Zhuang H, Singh A, Hennig R. Computational discovery of single-layer III–V materials. *Phys Rev B*. 2013;87:165415.
82. Norouzi S, Shahtahmassebi N, Behdani M, Roknabadi MR. High piezoelectricity in the buckled V-structure monolayers of group III–V: an Ab initio calculation. *Physica E*. 2018;102: 88-94.
83. Sante DD, Stroppa A, Barone P, Whangbo MH, Picozzi S. Emergence of ferroelectricity and spin-valley properties in two-dimensional honeycomb binary compounds. *Phys Rev B*. 2015;91:161401.
84. Shi J, Han C, Wang X, Yun S. Electronic, elastic and piezoelectric properties of boron-V group binary and ternary monolayers. *Phys B Condens Matter*. 2019;574:311634.
85. Gao R, Gao Y. Piezoelectricity in two-dimensional group III-V buckled honeycomb monolayers. *Phys Status Solidi Rapid Res Lett*. 2017;11:1600412.
86. Şahin H, Cahangirov S, Topsakal M, et al. Monolayer honeycomb structures of group-IV elements and III–V binary compounds: first-principles calculations. *Phys Rev B*. 2009;80: 155453.
87. Peng YY, Lu JF, Peng DF, et al. Dynamically modulated GaN whispering gallery Llasing mode for strain sensor. *Adv Funct Mater*. 2019;29:1905051.
88. Li X, Chen M, Yu R, et al. Enhancing light emission of ZnO-nanofilm/Si-micropillar heterostructure arrays by piezo-phototronic effect. *Adv Mater*. 2015;27:4447-4453.
89. Li W, Li J. Piezoelectricity in two-dimensional group-III monochalcogenides. *Nano Res*. 2015;8:3796-3802.
90. Li YH, Yu CB, Li Z, et al. Layer-dependent and light-tunable surface potential of two-dimensional indium selenide (InSe) flakes. *Rare Metals*. 2020;39:1356-1363.
91. Guo Y, Zhou S, Bai Y, Zhao J. Enhanced piezoelectric effect in Janus group-III chalcogenide monolayers. *Appl Phys Lett*. 2017;110:163102.
92. Li R, Cheng Y, Huang W. Recent progress of Janus 2D transition metal chalcogenides: from theory to experiments. *Small*. 2018;14:e1802091.
93. Li L, Chen Z, Hu Y, et al. Single-layer single-crystalline SnSe nanosheets. *J Am Chem Soc*. 2013;135:1213-1216.
94. Fei R, Li W, Li J, Yang L. Giant piezoelectricity of monolayer group IV monochalcogenides: SnSe, SnS, GeSe, and GeS. *Appl Phys Lett*. 2015;107:173104.
95. Li L, Han W, Pi L, et al. Emerging in-plane anisotropic two-dimensional materials. *InfoMat*. 2019;1:54-73.
96. Hu T, Dong J. Two new phases of monolayer group-IV monochalcogenides and their piezoelectric properties. *Phys Chem Chem Phys*. 2016;18:32514-32520.
97. Tan CG, Zhou P, Lin JG, Sun LZ. Two-dimensional semiconductors XY 2 (X = Ge, Sn; Y = S, Se) with promising piezoelectric properties. *Comput Condens Matter*. 2017;11:33-39.
98. Yin H, Gao J, Zheng GP, Wang Y, Ma Y. Giant piezoelectric effects in monolayer group-V binary compounds with honeycomb phases: a first-principles prediction. *J Phys Chem C*. 2017;121:25576-25584.

99. Zelisko M, Hanlumyuang Y, Yang S, et al. Anomalous piezoelectricity in two-dimensional graphene nitride nanosheets. *Nat Commun*. 2014;5:4284.
100. Kim JH, Kweon SH, Nahm S. Low-temperature crystalline lead-free piezoelectric thin films grown on 2D perovskite nanosheet for flexible electronic device applications. *Nano Res*. 2019;12:2559-2567.
101. Shi Z, Cao R, Khan K, et al. Two-dimensional tellurium: progress, challenges, and prospects. *Nano-Micro Lett*. 2020;12:99.
102. Yin H, Zheng GP, Gao J, Wang Y, Ma Y. Enhanced piezoelectricity of monolayer phosphorene oxides: a theoretical study. *Phys Chem Chem Phys*. 2017;19:27508-27515.
103. Zhou Y, Wu D, Zhu Y, et al. Out-of-plane piezoelectricity and ferroelectricity in layered α-In_2Se_3 nanoflakes. *Nano Lett*. 2017;17:5508-5513.
104. Zhao K, Guo Y, Shen Y, Wang Q, Kawazoe Y, Jena P. Penta-BCN: a new ternary pentagonal monolayer with intrinsic piezoelectricity. *J Phys Chem Lett*. 2020;11:3501-3509.
105. Ahammed R, Jena N, Rawat A, Mohanta MK, Dimple, De Sarkar A. Ultrahigh out-of-plane piezoelectricity meets giant Rashba effect in 2D Janus monolayers and bilayers of group IV transition-metal trichalcogenides. *J Phys Chem C*. 2020;124:21250-21260.
106. Cheon G, Duerloo KAN, Sendek AD, Porter C, Chen Y, Reed EJ. Data mining for new two- and one-dimensional weakly bonded solids and lattice-commensurate heterostructures. *Nano Lett*. 2017;17:1915-1923.
107. Liu H, Chen X, Zheng Y, et al. Lightweight, superelastic, and hydrophobic polyimide nanofiber/MXene composite aerogel for wearable piezoresistive sensor and oil/water separation applications. *Adv Funct Mater*. 2021;31:2008006.
108. He J, Xiao P, Lu W, et al. A universal high accuracy wearable pulse monitoring system via high sensitivity and large linearity graphene pressure sensor. *Nano Energy*. 2019;59:422-433.
109. Peng D, Liu X, Pan CF. Epitaxial lift-off for controllable single-crystalline perovskites. *Sci Bull*. 2021;66:6-8.
110. Chhowalla M, Shin HS, Eda G, Li LJ, Loh KP, Zhang H. The chemistry of two-dimensional layered transition metal dichalcogenide nanosheets. *Nat Chem*. 2013;5:263-275.
111. Rasmussen FA, Thygesen KS. Computational 2D materials database: electronic structure of transition-metal dichalcogenides and oxides. *J Phys Chem C*. 2015;119:13169-13183.
112. Dimple, Rawat A, Ahammed R, Mohanta MK, Sarkar AD, Jena N. Emergence of high piezoelectricity along with robust electron mobility in janus structures in semiconducting group IVB dichalcogenide monolayers. *J Mater Chem A*. 2018;6:24885-24898.
113. Yu W, Niu C-Y, Zhu Z, Wang X, Zhang W-B. Atomically thin binary V-V compound semiconductor: a first-principles study. *J Mater Chem C*. 2016;4:6581-6587.
114. Rodrigues GC, Zelenovskiy P, Romanyuk K, Luchkin S, Kopelevich Y, Kholkin A. Strong piezoelectricity in single-layer graphene deposited on SiO_2 grating substrates. *Nat Commun*. 2015;6:7572.
115. Ong MT, Duerloo KAN, Reed EJ. The effect of hydrogen and fluorine coadsorption on the piezoelectric properties of graphene. *J Phys Chem C*. 2013;117:3615-3620.
116. Ong MT, Reed EJ. Engineered piezoelectricity in graphene. *ACS Nano*. 2012;6:1387-1394.
117. Allouche A, Ferro Y, Angot T, Thomas C, Layet JM. Hydrogen adsorption on graphite (0001) surface: a combined spectroscopy-density-functional-theory study. *J Chem Phys*. 2005;123:124701.
118. El-Kelany KE, Carbonnière P, Erba A, Rérat M. Inducing a finite in-plane piezoelectricity in graphene with low concentration of inversion symmetry-breaking defects. *J Phys Chem C*. 2015;119:8966-8973.
119. Hu T, Hong J. First-principles study of metal adatom adsorption on black phosphorene. *J Phys Chem C*. 2015;119:8199-8207.
120. Kim HJ, Noor-A-Alam M, Son JY, Shin YH. Origin of piezoelectricity in monolayer halogenated graphane piezoelectrics. *Chem Phys Lett*. 2014;603:62-66.
121. Nair RR, Ren W, Jalil R, et al. Fluorographene: a two-dimensional counterpart of teflon. *Small*. 2010;6:2877-2884.
122. Robinson JT, Burgess JS, Junkermeier CE, et al. Properties of fluorinated graphene films. *Nano Lett*. 2010;10:3001-3005.
123. Chandratre S, Sharma P. Coaxing graphene to be piezoelectric. *Appl Phys Lett*. 2012;100:023114.
124. Faccio R, Fernandez-Werner L, Pardo H, Goyenola C, Ventura ON, Mombru AW. Electronic and structural distortions in graphene induced by carbon vacancies and boron doping. *J Phys Chem C*. 2010;114:18961-18971.
125. Dou L, Wong AB, Yu Y, et al. Atomically thin two-dimensional organic-inorganic hybrid perovskites. *Science*. 2015;349:1518-1521.
126. Du KZ, Tu Q, Zhang X, et al. Two-dimensional lead (II) halide-based hybrid perovskites templated by acene alkylamines: crystal structures, optical properties, and piezoelectricity. *Inorg Chem*. 2017;56:9291-9302.
127. Chen X, Song X, Zhang Z, et al. Two-dimensional layered perovskite ferroelectric with giant piezoelectric voltage coefficient. *J Am Chem Soc*. 2020;142:1077-1082.
128. Shao CR, Hu W. Lateral epitaxial grown of two-dimensional halide perovskite heterostructures. *Rare Metals*. 2020;39:863-864.
129. Liu J, Xue Y, Wang Z, et al. Two-dimensional $CH_3NH_3PbI_3$ perovskite: synthesis and optoelectronic application. *ACS Nano*. 2016;10:3536-3542.
130. Li F, Pan CF, Gong Y, et al. High Br- content $CsPb(Cl_yBr_{1-y})_3$ perovskite nanocrystals with strong Mn^{2+} emission through diverse cation/anion exchange engineering. *ACS Appl Mater Interfaces*. 2018;10:11739-11746.
131. Xia K, Wu WQ, Zhu MJ, et al. CVD growth of perovskite/graphene films for high-performance flexible image sensor. *Sci Bull*. 2020;65:343-349.
132. Li F, Lu J, Zhang Q, et al. Controlled fabrication, lasing behavior and excitonic recombination dynamics in single crystal $CH_3NH_3PbBr_3$ perovskite cuboids. *Sci Bull*. 2019;64:698-704.
133. Wu W, Wang X, Han X, et al. Flexible photodetector arrays based on patterned $CH_3NH_3PbI_{3-x}Cl_x$ perovskite film for real-time photosensing and imaging. *Adv Mater*. 2019;31:e1805913.
134. Zhang G, Huang S, Chaves A, et al. Infrared fingerprints of few-layer black phosphorus. *Nat Commun*. 2017;8:14071.

135. Island JO, Kuc A, Diependaal EH, et al. Precise and reversible band gap tuning in single-layer $MoSe_2$ by uniaxial strain. *Nanoscale*. 2016;8:2589-2593.
136. Zhu C, Wang G, Liu B, et al. Strain tuning of optical emission energy and polarization in monolayer and bilayer MoS_2. *Phys Rev B*. 2013;88:121301.
137. Zhu H, Wang Y, Xiao J, et al. Observation of piezoelectricity in free-standing monolayer MoS_2. *Nat Nanotechnol*. 2015;10:151-155.
138. Qi J, Lan YW, Stieg AZ, et al. Piezoelectric effect in chemical vapour deposition-grown atomic-monolayer triangular molybdenum disulfide piezotronics. *Nat Commun*. 2015;6:7430.
139. Manzeli S, Allain A, Ghadimi A, Kis A. Piezoresistivity and strain-induced band gap tuning in atomically thin MoS_2. *Nano Lett*. 2015;15:5330-5335.
140. Li Y, Xu CY, Zhen L. Surface potential and interlayer screening effects of few-layer MoS_2 nanoflakes. *Appl Phys Lett*. 2013;102:143110.
141. Castellanos-Gomez A, Poot M, Steele GA, Van der Zant HSJ, Agraït N, Rubio-Bollinger G. Elastic properties of freely suspended MoS_2 nanosheets. *Adv Mater*. 2012;24:772-775.
142. Brennan CJ, Ghosh R, Kou KL, Banerjee SK, Lu N, Yu ET. Out-of-plane electromechanical response of monolayer molybdenum disulfide measured by piezoresponse force microscopy. *Nano Lett*. 2017;17:5464-5471.
143. Kim SK, Bhatia R, Kim TH, et al. Directional dependent piezoelectric effect in CVD grown monolayer MoS_2 for flexible piezoelectric nanogenerators. *Nano Energy*. 2016;22:483-489.
144. Soergel E. Piezoresponse force microscopy (PFM). *J Phys D Appl Phys*. 2011;44:464003.
145. Wang X, He X, Zhu H, et al. Subatomic deformation driven by vertical piezoelectricity from CdS ultrathin films. *Sci Adv*. 2016;2:e1600209.
146. Wang Y, Vu LM, Lu T, et al. Piezoelectric responses of mechanically exfoliated two-dimensional SnS_2 nanosheets. *ACS Appl Mater Interfaces*. 2020;12:51662-51668.
147. Jin HJ, Yoon WY, Jo W. Virtual out-of-plane piezoelectric response in MoS_2 layers controlled by ferroelectric polarization. *ACS Appl Mater Interfaces*. 2018;10:1334-1339.
148. Gruverman A, Alexe M, Meie D. Piezoresponse force microscopy and nanoferroic phenomena. *Nat Commun*. 2019;10:1661.
149. Esfahani EN, Li T, Huang B, Xu X, Li J. Piezoelectricity of atomically thin WSe_2 via laterally excited scanning probe microscopy. *Nano Energy*. 2018;52:117-122.
150. Li X, Collins L, Miyazawa K, Fukuma T, Jesse S, Kalinin SV. High-veracity functional imaging in scanning probemicroscopy via graph-bootstrapping. *Nat Commun*. 2018;9:2428.
151. Liu B, Chen L, Liu G, Abbas AN, Fathi M, Zhou C. High-performance chemical sensing using Schottky-contacted chemical vapor deposition grown monolayer MoS_2 transistors. *ACS Nano*. 2014;8:5304-5314.
152. Shanmugam M, Durcan CA, Yu B. Layered semiconductor molybdenum disulfide nanomembrane based Schottky-barrier solar cells. *Nanoscale*. 2012;4:7399-7405.
153. Zhang Y, Liu Y, Wang ZL. Fundamental theory of piezotronics. *Adv Mater*. 2011;23:3004-3013.
154. Zhou R, Hu C, Yu R, Pan C, Wang ZL. Piezotronic effect enhanced detection of flammable/toxic gases by ZnO micro/-nanowire sensors. *Nano Energy*. 2015;12:588-596.
155. Pan C, Zhai J, Wang ZL. Piezotronics and piezo-phototronics of third generation semiconductor nanowires. *Chem Rev*. 2019;119:9303-9359.
156. Zhang K, Peng M, Wu W, et al. A flexible p-CuO/n-MoS_2 heterojunction photodetector with enhanced photoresponse by the piezo-phototronic effect. *Mater Horizons*. 2017;4:274-280.
157. Xue F, Chen L, Chen J, et al. P-type MoS_2 and n-type ZnO diode and its performance enhancement by the piezophototronic effect. *Adv Mater*. 2016;28:3391-3398.
158. Wang ZL, Wu W. Piezotronics and piezo-phototronics: fundamentals and applications. *Natl Sci Rev*. 2014;1:62-90.
159. Hua Q, Sun J, Liu H, et al. Skin-inspired highly stretchable and conformable matrix networks for multifunctional sensing. *Nat Commun*. 2018;9:244.
160. Arsat R, Breedon M, Shafiei M, et al. Graphene-like nanosheets for surface acoustic wave gas sensor applications. *Chem Phys Lett*. 2009;467:344-347.
161. Long M, Gao A, Wang P, et al. Room temperature high-detectivity mid-infrared photodetectors based on black arsenic phosphorus. *Sci Adv*. 2017;3:1700589.
162. Dai M, Zheng W, Zhang X, et al. Enhanced piezoelectric effect derived from grain boundary in MoS_2 monolayers. *Nano Lett*. 2020;20:201-207.
163. Feng W, Zheng W, Gao F, et al. Sensitive electronic-skin strain sensor array based on the patterned two-dimensional α-In_2Se_3. *Chem Mater*. 2016;28:4278-4283.
164. Wang L, Liu S, Gao G, et al. Ultrathin piezotronic transistors with 2 nm channel lengths. *ACS Nano*. 2018;12:4903-4908.
165. Pang Y, Yang Z, Yang Y, Ren T. Wearable electronics based on 2D materials for human physiological information detection. *Small*. 2020;16:e1901124.
166. Guo J, Wen R, Zhai J, Wang ZL. Enhanced NO_2 gas sensing of a single-layer MoS_2 by photogating and piezo-phototronic effects. *Sci Bull*. 2019;64:128-135.
167. Zhang D, Yang Z, Li P, Pang M, Xue Q. Flexible self-powered high-performance ammonia sensor based on Au-decorated $MoSe_2$ nanoflowers driven by single layer MoS_2-flake piezoelectric nanogenerator. *Nano Energy*. 2019;65:103974.
168. Wang Y, Zhu W, Deng Y, et al. Self-powered wearable pressure sensing system for continuous healthcare monitoring enabled by flexible thin-film thermoelectric generator. *Nano Energy*. 2020;73:104773.
169. Schwartz G, Tee BC, Mei J, et al. Flexible polymer transistors with high pressure sensitivity for application in electronic skin and health monitoring. *Nat Commun*. 2013;4:1859.
170. Dai M, Wang Z, Wang F, et al. Two-dimensional van der Waals materials with aligned in-plane polarization and large piezoelectric effect for self-powered piezoelectric sensors. *Nano Lett*. 2019;19:5410-5416.
171. Lin P, Zhu L, Li D, Wang ZL. Defect repair for enhanced piezo-phototronic MoS_2 flexible phototransistors. *J Mater Chem C*. 2019;7:14731-14738.
172. Du J, Liao Q, Hong M, et al. Piezotronic effect on interfacial charge modulation in mixed-dimensional van der Waals heterostructure for ultrasensitive flexible photodetectors. *Nano Energy*. 2019;58:85-93.

173. Hou P, Lv Y, Chen Y, et al. In-plane strain-modulated photoresponsivity of the α-In_2Se_3 based flexible transistor. *ACS Appl Electron Mater*. 2019;2:140-146.
174. Dai M, Chen H, Wang F, et al. Robust piezo-phototronic effect in multilayer γ-InSe for high-performance self-powered flexible photodetectors. *ACS Nano*. 2019;13:7291-7299.
175. Inbaraj CRP, Mathew RJ, Haider G, et al. Ultra-high performance flexible piezopotential gated $In_{1-x}Sn_xSe$ phototransistor. *Nanoscale*. 2018;10:18642-18650.
176. Zhang K, Zhai J, Wang ZL. A monolayer MoS_2 p-n homogenous photodiode with enhanced photoresponse by piezo-phototronic effect. *2D Mater*. 2018;5:035038.
177. Lin P, Zhu L, Li D, Xu L, Pan C, Wang ZL. Piezo-phototronic effect for enhanced flexible MoS_2/WSe_2 van der Waals photodiodes. *Adv Funct Mater*. 2018;28:1802849.
178. Guo J, Wen R, Liu Y, et al. Piezotronic effect enhanced flexible humidity sensing of monolayer MoS_2. *ACS Appl Mater Interfaces*. 2018;10:8110-8116.
179. Liu H, Li Q, Bu Y, et al. Stretchable conductive nonwoven fabrics with self-cleaning capability for tunable wearable strain sensor. *Nano Energy*. 2019;66:104143.
180. Zhou K, Zhao Y, Sun X, et al. Ultra-stretchable triboelectric nanogenerator as high-sensitive and self-powered electronic skins for energy harvesting and tactile sensing. *Nano Energy*. 2020;70:104546.
181. Wang CC, Pan CF, Wang ZL. Electronic skin for closed-loop systems. *ACS Nano*. 2019;13:12287-12293.
182. Han SA, Lee J, Lin J, Kim SW, Kim JH. Piezo/triboelectric nanogenerators based on 2-dimensional layered structure materials. *Nano Energy*. 2019;57:680-691.
183. Zhou Y, Liu W, Huang X, Zhang A, Zhang Y, Wang ZL. Theoretical study on two-dimensional MoS_2 piezoelectric nanogenerators. *Nano Res*. 2016;9:800-807.
184. Wang ZL. On Maxwell's displacement current for energy and sensors: the origin of nanogenerators. *Mater Today*. 2017;20:74-82.
185. Wang ZL. Towards self-powered nanosystems: from nanogenerators to nanopiezotronics. *Adv Funct Mater*. 2008;18:3553-3567.
186. Han JK, Kim S, Jang S, et al. Tunable piezoelectric nanogenerators using flexoelectricity of well-ordered hollow 2D MoS_2 shells arrays for energy harvesting. *Nano Energy*. 2019;61:471-477.
187. Lee GJ, Lee MK, Park JJ, Hyeon DY, Jeong CK, Park K. Piezoelectric energy harvesting from two-dimensional boron nitride nanoflakes. *ACS Appl Mater Interfaces*. 2019;11:37920-37926.
188. Chen J, Qiu Y, Yang D, She J, Wang Z. Improved piezoelectric performance of two-dimensional ZnO nanodisks-based flexible nanogengerators via ZnO/Spiro-MeOTAD PN junction. *J Mater Sci Mater El*. 2020;31:5584-5590.
189. Lee Y, Kim S, Kim D, Lee C, Park H, Lee JH. Direct-current flexible piezoelectric nanogenerators based on two-dimensional ZnO nanosheet. *Appl Surf Sci*. 2020;509:145328.
190. Verma K, Bharti DK, Badatya S, Srivastava AK, Gupta MK. High performance flexible two dimensional vertically aligned ZnO nanodisc based piezoelectric nanogenerator via surface passivation. *Nanoscale Adv*. 2020;2:2044-2051.
191. Lee JH, Park JY, Cho BE, et al. Reliable piezoelectricity in bilayer WSe_2 for piezoelectric nanogenerators. *Adv Mater*. 2017;29:1606667.
192. Feng J, Graf M. Liu k, et al. single-layer nanopores as nanopower generators. *Nature*. 2016;536:197-200.
193. Abbood HA, Alabadi A, Al-Hawash AB, Abbood AA, Huang K. Square CdS micro/nanosheets as efficient photo/piezo-bi-catalyst for hydrogen production. *Catal Lett*. 2020;150:3059-3070.
194. Li S, Zhao Z, Yu D, et al. Few-layer transition metal dichalcogenides (MoS_2, WS_2, and WSe_2) for water splitting and degradation of organic pollutants: understanding the piezocatalytic effect. *Nano Energy*. 2019;66:104083.
195. Chen Y, Deng X, Wen J, Zhu J, Bian Z. Piezo-promoted the generation of reactive oxygen species and the photodegradation of organic pollutants. *Appl Catal B Environ*. 2019;258:118024.
196. Yalagala B, Sahatiya P, Mattela V, Badhulika S. Ultra-low cost, large area graphene/MoS_2-based piezotronic memristor on paper: a systematic study for both direct current and alternating current inputs. *ACS Appl Electron Mater*. 2019;1:883-891.
197. Poh SM, Tan SJR, Wang H, et al. Molecular-beam epitaxy of two-dimensional In_2Se_3 and its giant electroresistance switching in ferroresistive memory junction. *Nano Lett*. 2018;18:6340-6346.
198. Strukov DB, Snider GS, Stewart DR, Williams RS. The missing memristor found. *Nature*. 2008;453:80-83.
199. Liu J, Zhang Z, Qiao S, Fu G, Wang S, Pan C. Lateral bipolar photoresistance effect in the CIGS heterojunction and its application in position sensitive detector and memory device. *Sci Bull*. 2020;65:477-485.
200. Hui YY, Liu X, Jie W, et al. Exceptional tunability of band energy in a compressively strained trilayer MoS_2 sheet. *ACS Nano*. 2013;7:7126-7131.
201. Yang S, Chen Y, Jiang C. Strain engineering of two-dimensional materials: methods, properties, and applications. *InfoMat*. 2021;3:397-420.
202. Chen JR, Odenthal PM, Swertz AG, et al. Control of Schottky barriers in single layer MoS_2 transistors with ferromagnetic contacts. *Nano Lett*. 2013;13:3106-3110.
203. Li Z, Lv Y, Ren L, et al. Efficient strain modulation of 2D materials via polymer encapsulation. *Nat Commun*. 2020;11:1151.
204. Conley HJ, Wang B, Ziegler JI, Haglund RF Jr, Pantelides ST, Bolotin KI. Bandgap engineering of strained monolayer and bilayer MoS_2. *Nano Lett*. 2013;13:3626-3630.
205. Ghorbani-Asl M, Borini S, Kuc A, Heine T. Strain-dependent modulation of conductivity in single-layer transition-metal dichalcogenides. *Phys Rev B*. 2013;87:235434.
206. Zhang J, Yu Y, Wang P, et al. Characterization of atomic defects on the photoluminescence in two-dimensional materials using transmission electron microscope. *InfoMat*. 2019;1:85-97.
207. Rhodes D, Chae SH, Ribeiro-Palau R, Hone J. Disorder in van der Waals heterostructures of 2D materials. *Nat Mater*. 2019;18:541-549.
208. Lin Z, Carvalho BR, Kahn E, et al. Defect engineering of two-dimensional transition metal dichalcogenides. *2D Mater*. 2016;3:022002.
209. Wang S, Robertson A, Warner JH. Atomic structure of defects and dopants in 2D layered transition metal dichalcogenides. *Chem Soc Rev*. 2018;47:6764-6794.

210. Zhang X, Liao Q, Liu S, et al. Poly(4-styrenesulfonate)-induced sulfur vacancy self-healing strategy for monolayer MoS_2 homojunction photodiode. *Nat Commun*. 2017;8:15881.
211. Gao L, Liao Q, Zhang X, et al. Defect-engineered atomically thin MoS_2 homogeneous electronics for logic inverters. *Adv Mater*. 2020;32:1906646.
212. Ghorbani-Asl M, Enyashin AN, Kuc A, Seifert G, Heine T. Defect-induced conductivity anisotropy in MoS_2 monolayers. *Phys Rev B*. 2013;88:245440.
213. Ma PW, Dudarev SL. Effect of stress on vacancy formation and migration in body-centered-cubic metals. *Phys Rev Mater*. 2019;3:063601.
214. Souza RAD, Ramadan A, Horner S. Modifying the barriers for oxygen-vacancy migration in fluorite-structured CeO_2 electrolytes through strain: a computer simulation study. *Energ Environ Sci*. 2012;5:5445-5453.
215. Tsai C, Park S, Park J, et al. Electrochemical generation of sulfur vacancies in the basal plane of MoS_2 for hydrogen evolution. *Nat Commun*. 2017;8:15113.
216. Komsa HP, Kurasch S, Lehtinen O, Kaiser U, Krasheninnikov AV. From point to extended defects in two-dimensional MoS_2: evolution of atomic structure under electron irradiation. *Phys Rev B*. 2013;88:035301.
217. Musca CA, Dell JM, Faraone L, et al. Analysis of crosstalk in HgCdTe p-on-n heterojunction photovoltaic infrared sensing arrays. *Electron Mater*. 1999;28:617-623.
218. Huo Z, Peng Y, Zhang Y, et al. Recent advances in large-scale tactile sensor arrays based on a transistor matrix. *Adv Mater Interfaces*. 2018;5:1801061.
219. Andresen BF, Shtrichman I, Fulop GF, et al. Spatial resolution of SCD's InSb 2D detector arrays. *Infrared Technol Appl XXXIII*. 2007;6542:65423M.
220. Lin W, Wang B, Peng G, Shan Y, Hu H, Yang Z. Skin-inspired piezoelectric tactile sensor array with crosstalk-free row+column electrodes for spatiotemporally distinguishing diverse stimuli. *Adv Sci*. 2021;8:2002817.

AUTHOR BIOGRAPHIES

Qin Zhang received her BS degree (2018) in Materials Science and Engineering from Jingdezhen Ceramic Institute, China. She is currently a graduate student at School of Physical Science and Technology in Guangxi University. Her main research direction is the microscopic mechanism and applications of 2D flexible devices.

Ping Chen received her BS degree (2011) and PhD (2016) in Materials Science and Engineering from Central South University and Zhejiang University, China, respectively. She visited Sialon group at National Institute for Materials Science in Japan from 2015 to 2016 as a visiting scholar. She is currently an associated professor at School of Physical Science and Technology in Guangxi University. Then, she joined the group of professors Zhong-Lin Wang and Cao-Feng Pan as a visiting scholar at Beijing Institute of Nanoenergy and Nanosystems, Chinese Academy of Sciences since 2018. Her main research is focused on optoelectronics devices of two-dimensional materials and fields modulating luminescence from lanthanide ions.

Caofeng Pan received his BS degree (2005) and his PhD (2010) in Materials Science and Engineering from Tsinghua University, China. He then joined the Georgia Institute of Technology as a postdoctoral fellow. He is currently a professor and a group leader at Beijing Institute of Nanoenergy and Nanosystems, Chines Academy of Sciences since 2013. His main research interests focus on the fields of pizotronics/piezo-phototronics for fabricating new electronic and optoelectronic devices, and self-powered nanosystems. Details can be found at http://www.piezotronics.cn

How to cite this article: Zhang Q, Zuo S, Chen P, Pan C. Piezotronics in two-dimensional materials. *InfoMat*. 2021;3(9):987–1007. https://doi.org/10.1002/inf2.12220